

Flow Around a Simplified Car Body (AHMED BODY): Description of Numerical Methodology

B. Basara¹, S. Jakirlic²

¹AVL List GmbH, Advanced Simulation Technologies, Graz, Austria

²Darmstadt University of Technology, Germany

1. NUMERICAL METHOD

The Computational Fluid Dynamics (CFD) code AVL SWIFT is used for the present simulations. The code employs the finite volume discretization method, which rests on the integral form of the general conservation law applied to the polyhedral control volumes (cells). The integral form can be written as:

$$\underbrace{\frac{d}{dt} \int_V \rho \phi dV}_{\text{Rate of change: } R} + \underbrace{\oint_A \rho \phi U_k dA_k}_{\text{Convection: } C} = \underbrace{\oint_A \Gamma_\phi^{kk} \frac{\partial \phi}{\partial x_k} dA_k}_{\text{Diffusion: } D} + \underbrace{\int_V s_\phi^V dV + \oint_A s_{\phi k}^A dA_k}_{\text{Sources: } S} . \quad (1)$$

where a general variable $\phi(x_k, t)$ can represent either scalars or vector and tensor field components. Here, the Cartesian coordinate system (x, y, z) with the unit vectors $(\vec{i}, \vec{j}, \vec{k})$ is used and tensor notation is employed. In the above equation, ρ is the fluid density, t is time, U_k are components of the fluid velocity vector, Γ_ϕ^{kk} is the diffusion coefficient for the variable ϕ (in this case repeated indices don't imply summation), s_ϕ^V and $s_{\phi k}^A$ are the volumetric and surface source terms, respectively.

All dependent variables are stored at the geometric centre of the control volume. The appropriate data structure (cell-face based connectivity) and interpolation practices for gradients and cell-face values are introduced to accommodate an arbitrary number of cell faces. The convection can be approximated by a variety of differencing schemes. The second order accurate and bounded MINMOD scheme is employed for this study (Przulj and Basara (2001)). The diffusion is approximated using central differencing. The overall solution procedure is iterative and is based on the SIMPLE-like segregated algorithm which ensures coupling between the velocity and pressure fields.

2. MODELLING EQUATIONS

The flow field is modelled by the ensemble-mean Navier Stokes equations coupled either with the eddy-viscosity $k - \varepsilon$ model equations or with the differential Reynolds stress model equations or with the both of these models fixed in the frame of hybrid turbulence model

presented below. The ensemble-mean momentum equations are recovered from Eq. (1) by setting $\phi = U_i$, $s_{\phi k}^A = \mu(\partial U_k / \partial x_i) - p\delta_{ik} - \rho\overline{u_i u_k}$ and $s_\phi^V = 0$, where μ is the dynamic viscosity, p is the pressure, δ_{ik} being the Kronecker delta and $\overline{u_i u_k}$ are unknown kinematic Reynolds stresses. For the mass conservation, one can formally set $\phi = 1$, $\Gamma_\phi^{kk} = s_{\phi k}^A = s_\phi^V = 0$.

2.1 The $k - \varepsilon$ model

In the $k - \varepsilon$ model of turbulence, the Reynolds stresses are obtained from the Boussinesq's eddy viscosity formulation:

$$-\rho\overline{u_i u_j} = -\frac{2}{3}\rho k\delta_{ij} + 2\mu_t S_{ij}, S_{ij} = \frac{1}{2}\left(\frac{\partial U_i}{\partial x_j} + \frac{\partial U_j}{\partial x_i}\right) \quad (2)$$

where k is the turbulent kinetic energy, S_{ij} is the mean rate of strain tensor and μ_t is the turbulent viscosity, which is evaluated from the expression:

$$\mu_t = \rho C_\mu \frac{k^2}{\varepsilon} \quad (3)$$

With reference to Eq. (1), the corresponding diffusion coefficients and source terms that describe the $k - \varepsilon$ model (ε being the dissipation rate of k by viscous action) are as follows:

$$\phi = k \Rightarrow \Gamma_\phi = \mu + \frac{\mu}{\sigma_k}, s_\phi^V = \rho(P_k - \varepsilon), s_{\phi k}^A = 0, P_k = -\overline{u_i u_j} \frac{\partial U_i}{\partial x_j} \quad (4)$$

$$\phi = \varepsilon \Rightarrow \Gamma_\phi = \mu + \frac{\mu_t}{\sigma_\varepsilon}, s_\phi^V = \rho(C_{\varepsilon 1}P_k - C_{\varepsilon 2}\varepsilon) \frac{\varepsilon}{k}, s_{\phi k}^A = 0 \quad (5)$$

where P_k is the production of the turbulent kinetic energy.

2.2 The Reynolds stress transport model (RSM)

In full second-order turbulence closures, the differential transport equations for the Reynolds stresses $\overline{u_i u_j}$ are solved. When closing these equations, the diffusion is modelled by a simple gradient transport hypothesis. The Reynolds stresses are represented by the integral Eq. (1) as:

$$\begin{aligned} \phi = \overline{u_i u_j}, \Rightarrow \Gamma_\phi^{kk} &= \mu + \rho C_s \frac{k}{\varepsilon} \overline{u_k u_k} \text{ (no summation on } k\text{)}, s_{\phi k}^A = \rho C_s \frac{k}{\varepsilon} \overline{u_k u_l} \frac{\partial \phi}{\partial x_l}, k \neq l \\ s_\phi^V &= \rho(P_{ij} - \varepsilon_{ij} + \Pi_{ij}), P_{ij} = -\overline{u_j u_k} \frac{\partial U_i}{\partial x_k} - \overline{u_i u_k} \frac{\partial U_j}{\partial x_k}, \varepsilon_{ij} = \frac{2}{3}\varepsilon\delta_{ij} \end{aligned} \quad (6)$$

where P_{ij} is the production by the mean velocity gradients, ε_{ij} denotes the dissipation rate tensor and Π_{ij} is the pressure-strain correlation. For the pressure-strain term, the SSG model of Speziale, Sarkar and Gatski (1991) is used. The SSG model does not require the use of wall-damping terms. This model is given as:

$$\begin{aligned}\Pi_{ij} = & -\left(C_1 \varepsilon + C_1^* P_k\right) b_{ij} + C_2 \varepsilon \left(b_{ik} b_{kj} - \frac{1}{3} b_{mn} b_{mn} \delta_{ij}\right) + \left(C_3 - C_3^* \sqrt{b_{mn} b_{mn}}\right) k S_{ij} \\ & + C_4 k \left(b_{ik} S_{jk} + b_{jk} S_{ik} - \frac{2}{3} b_{mn} S_{mn} \delta_{ij}\right) + C_5 k \left(b_{ik} W_{jk} + b_{jk} W_{ik}\right)\end{aligned}\quad (7)$$

where b_{ij} is the Reynolds stress anisotropy tensor and W_{ij} is the mean vorticity tensor. They are defined as:

$$b_{ij} = \frac{\overline{u_i u_j}}{2k} - \frac{1}{3} \delta_{ij}, \quad W_{ij} = \frac{1}{2} \left(\frac{\partial U_i}{\partial x_j} - \frac{\partial U_j}{\partial x_i} \right). \quad (8)$$

The ε -model equation, used in conjunction with the RSM model, has now the following diffusion coefficients and sources:

$$\begin{aligned}\phi = \varepsilon, \Rightarrow \Gamma_\phi^{kk} = & \mu + \rho C_\varepsilon \frac{k}{\varepsilon} \overline{u_k u_k} \text{ (no summation on } k), \\ s_{\phi k}^A = & \rho C_\varepsilon \frac{k}{\varepsilon} \overline{u_k u_l} \frac{\partial \varepsilon}{\partial x_l}, k \neq l, \quad s_\phi^V = \rho (C_{\varepsilon 1} P_k - C_{\varepsilon 2} \varepsilon) \frac{\varepsilon}{k}\end{aligned}\quad (9)$$

2.3 The hybrid turbulence model (HTM)

Although it has been shown in the past that the Reynolds-stress model (RSM) models can be used for real industrial applications, it is also inevitable that CFD users seek less complicated and more robust solutions. Seeking for such solution, Basara and Jakirlic (2001) and Basara, Jakirlic and Przulj (2001) recently proposed and validated a new and simpler scheme for turbulence models employment.

The $k - e$ models use the turbulence kinetic energy and its dissipation rate to define characteristic turbulence scales. The C_m coefficient is derived from the measured ratio $\overline{u_i u_j} / k$ for the wall boundary layers and then used as a constant value. With this assumption, the turbulence viscosity is determined and then used in momentum equations. A weak point of such formulation, beside its isotropic form, lies in a derivation of the constant C_m , which in reality does not vary just from one to another type of the flow but also across the same flow. Commonly used value is 0.09. An approach advanced by Basara and Jakirlic (2001) suggests a derivation of C_m by equalising the production of turbulence kinetic energy predicted by the Reynolds stress model and with the production obtained by the $k-\varepsilon$ model, thus

$$C_m = \frac{\overline{u_i u_j} \frac{\partial U_i}{\partial x_j} \frac{\partial U_j}{\partial x_i}}{\overline{u_i u_j} \frac{\partial \varepsilon}{\partial x_i}} = \frac{\overline{S_{ij} S_{ij}}}{\overline{S_{ij}}} \quad (10)$$

Therefore in proposed model, the stress and mean strain tensors are coupled via Boussinesq's formula, as in the standard $k-\varepsilon$ model. However, the turbulence kinetic energy is now obtained after solving full Reynolds stress transport equations. The dissipation rate equation is also solved in the form commonly used in the framework of the Reynolds-stress closures. Finally, the structural parameter C_m is calculated as a function given above rather than kept constant.

This ‘constant free’ eddy-viscosity model greatly improves results compared to its standard $k-\varepsilon$ counterpart. Several, very well-known weaknesses of the $k-\varepsilon$ modeling practice, pertinent especially to the rotating and swirling flows, separated flows, as well as flows with strong dilatational effects, are removed in such a way. On the other hand, this approach improves significantly the convergence rate in comparison to the Reynolds-stress model groups. Such formulation of the eddy viscosity model offers very robust computational procedure and accurate solutions.

It is clear that the hybrid turbulence model (HTM) is specifically designed to satisfy industrial needs. The first industrial meeting (AVL AST User Meeting 2001) where HTM was presented (Basara (2001)), showed that the industry has a high interest for such modelling practice. Therefore, the model is now intensively validated on a wide range of different flows, and this also includes a turbulent flow around Ahmed body.

3. COMPUTATIONAL GRID AND BOUNDARY CONDITIONS

The computational domain contains 523,000 hexahedral cells. Local grid refinement is applied (see Figure 1) to improve a grid resolution around the body. The grid is carefully checked for the numerical error by employing different differencing schemes and it represents the minimum size acceptable for turbulent models testing. For the full body, the grid size is 1 million which is also acceptable size for transient calculations. The first next to wall cells ensures y^+ values on the body to be less than 100. For 35 degree case, the grid is practically the same as one for 25 degree. Due attention was also given to the boundary conditions. Measured velocity profile was used for extrapolation at the inlet boundary faces. A minimum inlet distance from Ahmed Body has been validated and it was found that 0.5m is sufficient enough not to influence results. The best agreement was achieved when the inlet profile was taken from the same set of measurements used for comparisons (inlet profile was taken from $x=-1.443\text{m}$).

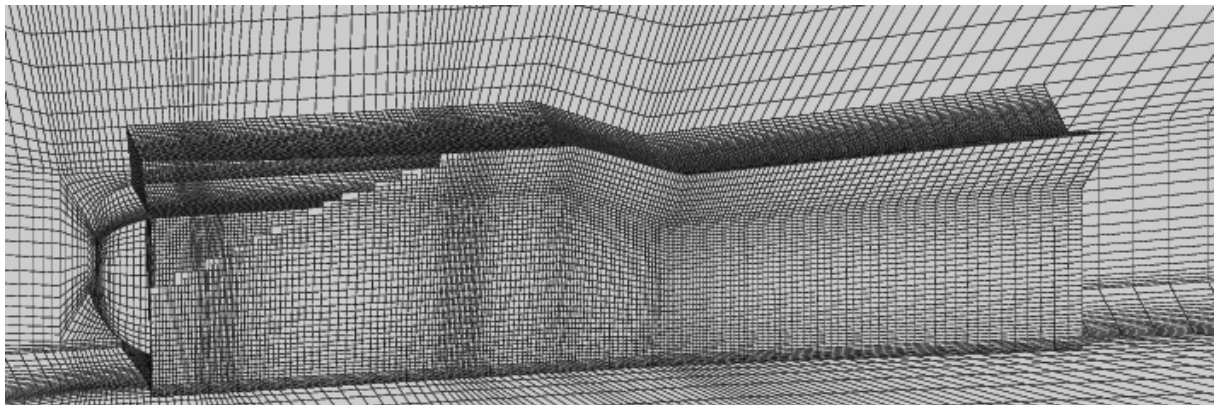


Figure 1: Calculation grid (523000 cells)

ACKNOWLEDGEMENTS. The authors are grateful to A. Basara for the help in post-processing of computational results.

REFERENCES

- (1) Basara, B. 2001, "Recent advances in AVL's CFD solvers: A quest towards unique solutions", AVL AST User Meeting, Graz, Austria.
 - (2) Basara, B., Jakirlic, S., 2001, "A New Turbulence Modeling Strategy For Industrial CFD", submitted for publication.
 - (3) Basara, B., Jakirlic, S., Przulj, V., 2001, "Vortex-Shedding Flows Computed Using a New, Hybrid Turbulence Model", The 8th Int. Symp. On Flow Modeling and Turbulence Measurements, Tokyo, Japan.
 - (4) Przulj, V., Basara, B., 2001, "Bounded Convection Schemes For Unstructured Grids", AIAA 2001-2593, Anaheim, USA.
 - (5) Speziale, C.G., Sarkar, S., and Gatski, T.B., 1991, "Modeling the Pressure-Strain Corellation of Turbulence – An Invariant Dynamical System Approach," Journal of Fluid Mechanics, Vol. 227, pp. 245-272.
- .

Simulation of flow around a simplified car body

E. Guilméneau & P. Queutey
Laboratoire de Mécanique des Fluides, CNRS UMR-6598
Division Modélisation Numérique
Ecole Centrale de Nantes
B.P. 92101, 44321 Nantes Cedex 3, France
E-Mail: Emmanuel.Guilmineau@ec-nantes.fr

1 Introduction

The study of three-dimensional flow around a ground vehicle has become a subject of significant importance in the automobile industry. One obvious way of improving the fuel economy of vehicles is to reduce aerodynamic drag by optimizing the body shape. Execution of good aerodynamic design under stylistic constraints requires an extensive understanding of the flow phenomena and, especially, how the aerodynamics are influenced by changes in body shape. The aerodynamic forces are caused by various viscous flow phenomena, such as the three-dimensional turbulent boundary layer on the body surface, longitudinal vortices induced by three-dimensional separation, recirculating flows caused by separation.

The flow region which presents the major contribution to a car's drag, and which poses severe problems to numerical predictions and experimental studies as well, is the wake flow behind the vehicle. The location at which the flow separates determines the size of the separation zone, and consequently the drag force. Clearly, a more exact simulation of the wake flow and of the separation process is essential for the accuracy of drag predictions. A real-life automobile is very complex shape to model or to study experimentally. However, the simplified vehicle shape employed by Ahmed [1] generates fully three-dimensional regions of separated flow which may enable a better understanding of such flows.

2 Code description

The ISIS code, developed by the DMN group, uses the unsteady incompressible Reynolds-Averaged-Navier-Stokes Equations (RANSE) written in a conservative form. The discretization scheme uses a finite-volume method, generalized to 2D, Axi and 3D unstructured meshes composed of control volumes of arbitrary shape. Flow variables share the same location at the center of control volume. A second-order accurate three-level fully implicit time discretization is used. The fluxes are evaluated using second-order accurate approximations [2]. The momentum and continuity equations are solved in a segregated way, using a SIMPLE-like algorithm based on the classical Rhie and Chow interpolations [3].

Presented results have been obtained with the steady RANSE and with a low-Reynolds turbulence model: the two-equations model of Menter (SST k- ω) [4].

3 Grid description

The computational domain is defined by the half body. It starts at one body length in front and five body lengths behind the Ahmed body. The width of the domain is 935 mm and the height is 1400 mm. The body is located at 50 mm above the plane. The mesh is generated by the software Gridgen.

The grid is composed to 2474237 mesh points with 37667 points on the Ahmed body. The number of cells is 3680100 with 2061543 hexahedral cells. Due to the low-Reynolds turbulence model, the distance between the first fluid points and the walls is fixed to 0.01 mm. Then, the distance y^+ is near to 1 for the Reynolds number considered ($Re = 2.784 \cdot 10^6$). Figure 1 shows a mesh view of the symmetric plane.

4 Results

The slant angle of 25° is only considered.

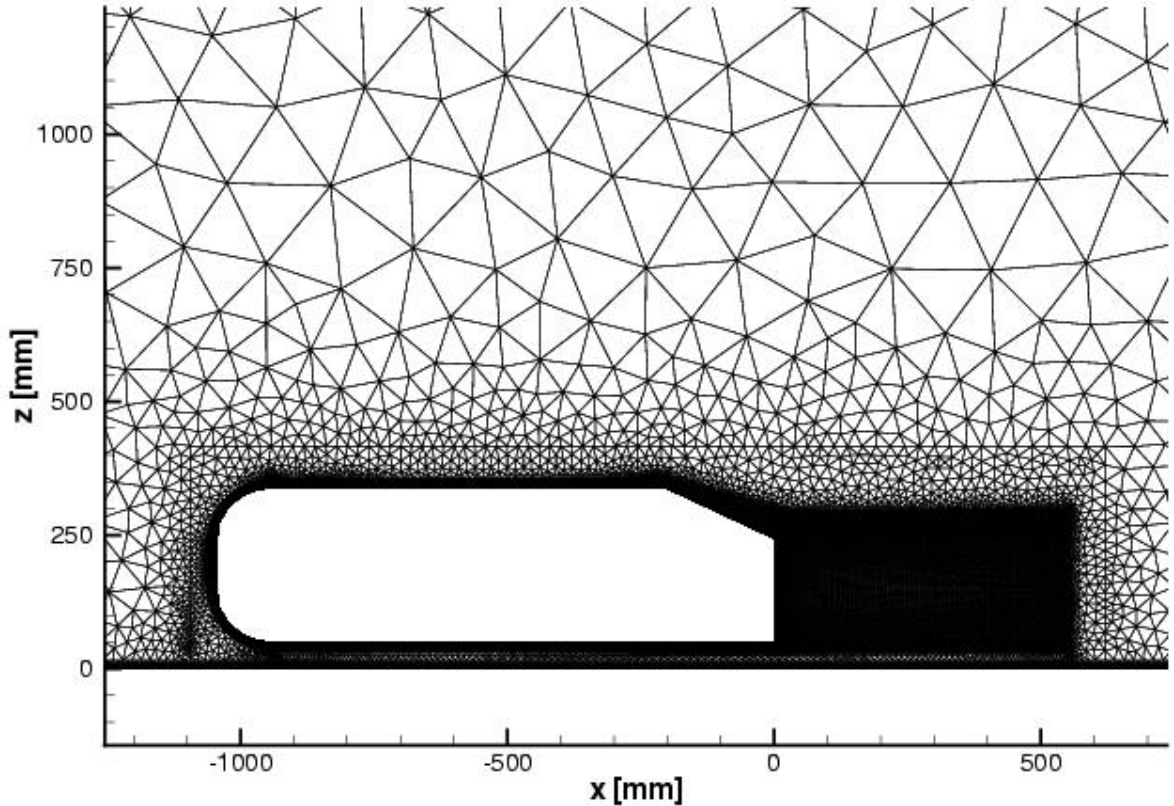


Figure 1: Mesh of the symmetric plane

The drag coefficient is 0.295. This value is close to the drag coefficient obtained in Ahmed *et al.* experiment [1] in which the drag coefficient is 0.285 with a Reynolds number of $4.29 \cdot 10^6$.

Figures 2 show a comparison of the streamline contours in the symmetric plane between experimental results 2(a) and numerical results 2(b). We can see that the vortices generated by the simulations are more intense than those produced in the experiments. The recirculation length is close to 200 mm in experiment 2(a) then in simulation, it is 300 mm 2(b).

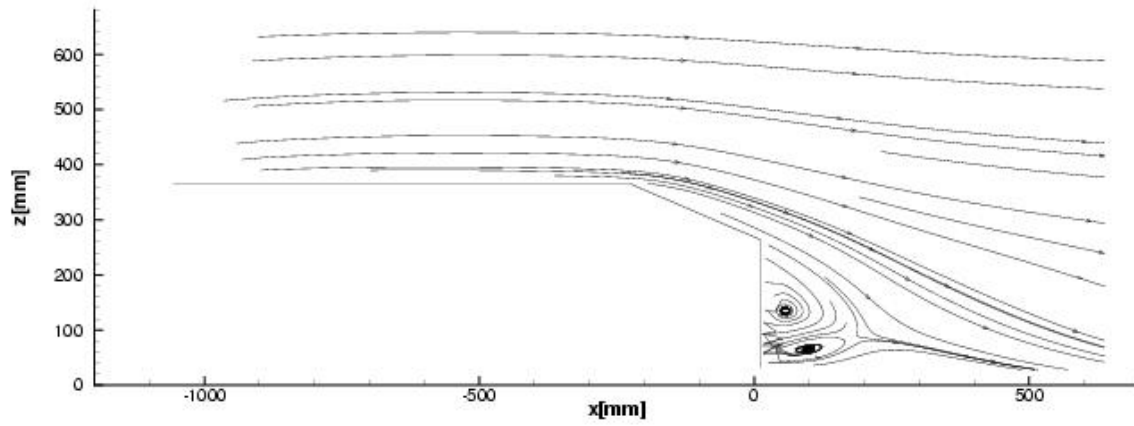
Figures 3 show the comparison of the streamline distributions between experimental results and numerical predictions in the one half of the symmetric planes at $x=0.080$ m, 0.200 m and 0.500 m. In figure 3(a), formation of the side vortex is visible. The flow behind the back of the body is different between experiment and simulation. At $x=0.200$ m, the concentration of streamlines is not located at the same position between numerical results and experiment results. At $x=0.500$ m, the recirculation is more concentrated in the computation results than in the experiments.

5 Conclusions

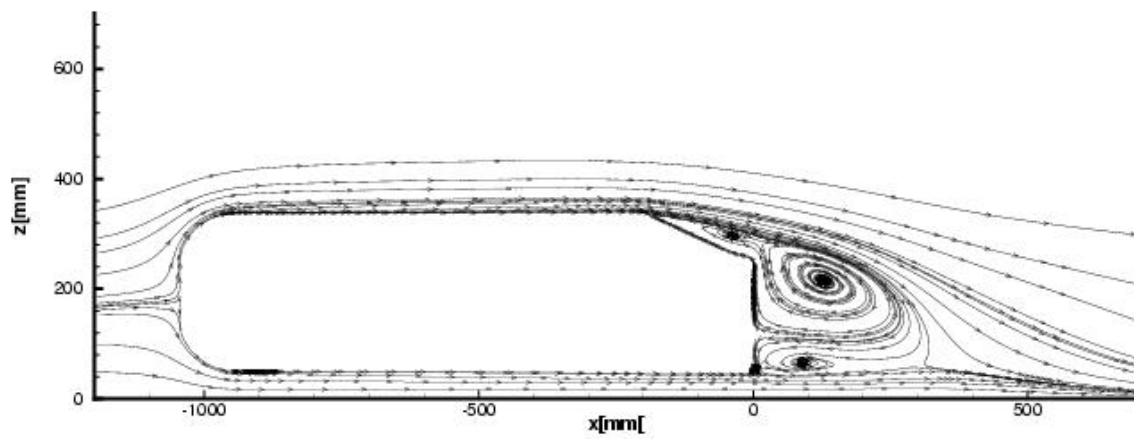
These results are preliminary results. We can notice that the simulation with the SST k- ω turbulence model predicts recirculation more intense. We must continue to study these configuration with others turbulence models, as Spalart-Allmaras, Rij- ω .

References

- [1] S. Ahmed, G. Ramm, and G. Faltin, “Some salient features of the time-averaged ground vehicle wake,” in *Society of Automotive Engineers*, SAE Paper 840300, 1984. [1](#) [2](#)
- [2] H. Jasak, H. Weller, and A. Gosman, “High resolution nvd differencing scheme for arbitrarily unstructured meshes,” *International Journal for Numerical Methods in Fluids*, vol. 31, pp. 431–449, 1999. [1](#)
- [3] C. Rhie and W. Chow, “A numerical study of the turbulent flow past an isolated aerofoil with trailing edge separation,” *AIAA Journal*, vol. 17, pp. 1525–1532, 1983. [1](#)



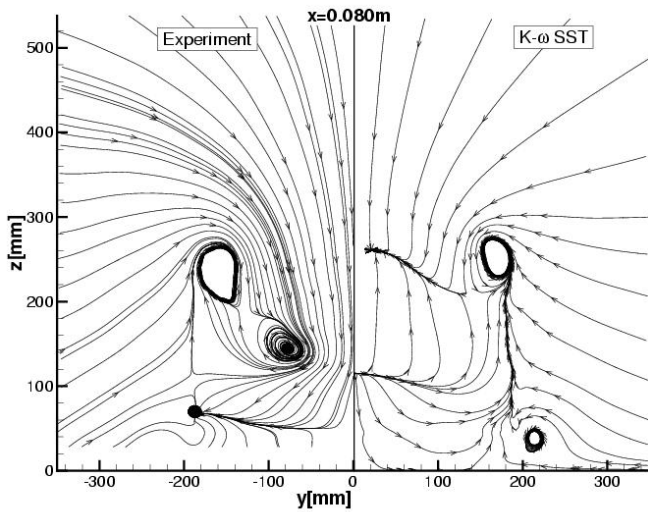
(a) Experiment



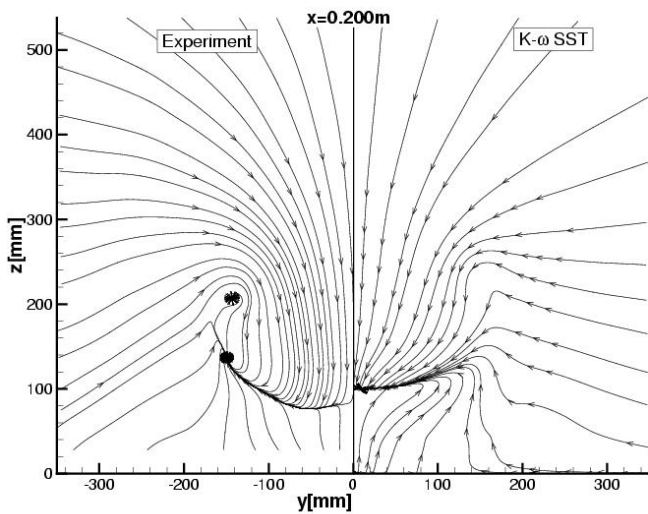
(b)

Figure 2: Streamline contours in the symmetric plane

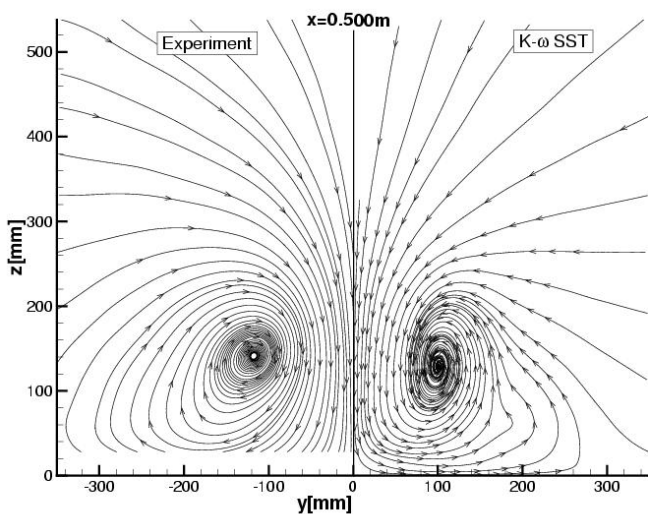
- [4] F. Menter, “Zonal two-equation $k - \omega$ turbulence models for aerodynamic flows,” in *AIAA 24th Fluid Dynamics Conference*, AIAA Paper 93-2906, (Orlando, U.S.A.), 1993. 1



(a) $x = 80 \text{ mm}$



(b) $x = 200 \text{ mm}$



(c) $x = 500 \text{ mm}$

Figure 3: Comparison of streamline contours in the one half of the symmetric transverse planes

Simulation of the Ahmed Body

Markus Braun, Marco Lanfrit
Fluent Deutschland GmbH
Hindenburgstr. 36
D-64295 Darmstadt

Davor Cokljat
Fluent Europe Ltd
Sheffield, UK

December 17, 2001

1 Introduction

External aerodynamics has always been of a great interest to automobile industry. Conducting experiments in wind tunnels gave ways to shape optimization and reduction of aerodynamic drag. During the eighties and nineties numerical simulations became more and more important due to their cost effectiveness. However, due to the lack of reliable turbulence models and lack of detailed data for validation, numerical simulations have never managed to replace experimental methods completely.

Detailed investigation of a simplified vehicle shape can be regarded as an important first step towards increasing reliability of existing solution tools. The experiments performed by Ahmed [1] and Lienhart et. al. [2] provided detailed experimental data that may be very useful in validating turbulence models for vehicle external aerodynamics.

2 Numerical Method

For the 9th ERCOFTAC/IAHR Workshop on Refined Turbulence Modeling several simulations have been performed with FLUENT in order to investigate the

flow around the Ahmed body. FLUENT is a commercial state-of-the-art CFD-code utilizing unstructured Control Volume method capable of dealing with all cell shapes including tetrahedron, hexahedron, prisms, pyramids and mixtures of them in hybrid grids. Compressible and incompressible variants of Reynolds Averaged Navier-Stokes (RANS) equations can be solved using a numerical method fully described in Mathur et. al. [3]. Several discretization schemes are available like first order upwind, power law, second-order upwind and QUICK.

For the computational results presented here FLUENT V6 has been employed.

3 Turbulence Modeling

FLUENT V6 provides a large suite of turbulence models within the context of RANS approach. Large Eddy Simulation is also available but due to practical reasons all simulations for this workshop have been performed using RANS based turbulence modeling. In that respect, two practical and relatively simple turbulence models have been adopted: the realizable $k - \epsilon$ model [4] and SST version of $k - \omega$ model [5]. Results obtained by these two models have been compared with experimental results from Lienhart and Becker [2].

Both models use the Boussinesq hypothesis to relate the Reynolds stresses to the mean velocity gradients:

$$-\rho \overline{u'_i u'_j} = \mu_t \left(\frac{\partial u_i}{\partial x_j} + \frac{\partial u_j}{\partial x_i} \right) - \frac{2}{3} \rho k \delta_{ij} \quad (1)$$

3.1 Realizable $k - \epsilon$ Model

The realizable $k - \epsilon$ model comes under two-equation group of models in which two additional transport equations for turbulence kinetic energy, k , and its rate of dissipation, ϵ , need to be solved in order to achieve closure:

$$\frac{\partial}{\partial t}(\rho k) + \frac{\partial}{\partial x_j}(\rho k u_j) = \frac{\partial}{\partial x_j} \left[\left(\mu + \frac{\mu_t}{\sigma_k} \right) \frac{\partial k}{\partial x_j} \right] + G_k - \rho \epsilon \quad (2)$$

$$\frac{\partial}{\partial t}(\rho \epsilon) + \frac{\partial}{\partial x_j}(\rho \epsilon u_j) = \frac{\partial}{\partial x_j} \left[\left(\mu + \frac{\mu_t}{\sigma_\epsilon} \right) \frac{\partial \epsilon}{\partial x_j} \right] + \rho C_1 S \epsilon - \rho C_2 \frac{\epsilon^2}{k + \sqrt{\nu \epsilon}}$$

where $C_1 = \max \left[0.43, \frac{\eta}{\eta+5} \right]$ and $\eta = S \frac{k}{\epsilon}$. In these equations, $G_k \equiv -\rho \overline{u'_i u'_j} \frac{\partial u_i}{\partial x_j}$ represents the generation of turbulence kinetic energy due to the mean velocity gradients and S is the mean strain rate.

The values for all constants in above equations have been set to the values as recommended in [4], namely $C_2 = 1.9$, $\sigma_k = 1$. and $\sigma_\epsilon = 1.2$.

3.1.1 Turbulent Viscosity

Turbulent viscosity μ_t is computed by combining k and ϵ as follows:

$$\mu_t = \rho C_\mu \frac{k^2}{\epsilon} \quad (3)$$

However, in the case of realizable $k - \epsilon$ model C_μ is no longer constant:

$$C_\mu = \frac{1}{A_0 + A_s \frac{kU^*}{\epsilon}} \quad (4)$$

where

$$U^* \equiv \sqrt{S_{ij}S_{ij} + \tilde{\Omega}_{ij}\tilde{\Omega}_{ij}} \quad (5)$$

and

$$\begin{aligned} \tilde{\Omega}_{ij} &= \Omega_{ij} - 2\epsilon_{ijk}\omega_k \\ \Omega_{ij} &= \overline{\Omega_{ij}} - \epsilon_{ijk}\omega_k \end{aligned}$$

where $\overline{\Omega_{ij}}$ is the mean rate-of-rotation tensor viewed in a rotating reference frame with the angular velocity ω_k . The model constants A_0 and A_s are given by

$$A_0 = 4.04, \quad A_s = \sqrt{6} \cos \phi$$

where

$$\begin{aligned} \phi &= \frac{1}{3} \cos^{-1}(\sqrt{6}W), \quad W = \frac{S_{ij}S_{jk}S_{ki}}{\tilde{S}}, \quad \tilde{S} = \sqrt{S_{ij}S_{ij}} \\ S_{ij} &= \frac{1}{2} \left(\frac{\partial u_j}{\partial x_i} + \frac{\partial u_i}{\partial x_j} \right) \end{aligned}$$

3.2 $k - \omega$ SST Model

The SST version of $k - \omega$ model also requires solution of two extra transport equations in order to achieve closure. In this case transport equations for turbulence kinetic energy, k , and specific dissipation rate, ω , are solved:

$$\frac{\partial}{\partial t}(\rho k) + \frac{\partial}{\partial x_j}(\rho k u_j) = \frac{\partial}{\partial x_j} \left[\left(\mu + \frac{\mu_t}{\sigma_k} \right) \frac{\partial k}{\partial x_j} \right] + G_k - \rho \beta^* k \omega \quad (6)$$

$$\frac{\partial}{\partial t}(\rho \omega) + \frac{\partial}{\partial x_j}(\rho \omega u_j) = \frac{\partial}{\partial x_j} \left[\left(\mu + \frac{\mu_t}{\sigma_\omega} \right) \frac{\partial \omega}{\partial x_j} \right] + G_\omega - \rho \beta \omega^2 + 2\rho(1 - F_1) \frac{1}{\sigma_{\omega,2}\omega} \frac{\partial k}{\partial x_j} \frac{\partial \omega}{\partial x_j} \quad (7)$$

where G_k and G_ω ($\equiv \frac{\gamma}{\nu_t} G_k$) stand for production of k and ω respectively. Turbulent Prandtl numbers σ_k and σ_ω are calculated as:

$$\sigma_k = \frac{1}{F_1/\sigma_{k,1} + (1 - F_1)/\sigma_{k,2}} \quad (8)$$

$$\sigma_\omega = \frac{1}{F_1/\sigma_{\omega,1} + (1 - F_1)/\sigma_{\omega,2}} \quad (9)$$

where constants are set to $\sigma_{k,1} = 1.176$, $\sigma_{\omega,1} = 2.0$, $\sigma_{k,2} = 1.0$, $\sigma_{\omega,2} = 1.168$. In above, F_1 is the blending function designed to blend model constants between wall affected region (subscript 1) and core turbulence region (subscript 2).

Constant β^* is equal to 0.09 in both regions while constant β is calculated as

$$\beta = F_1\beta_1 + (1 - F_1)\beta_2$$

whereby constant values in each region are set to $\beta_1 = 0.075$ $\beta_2 = 0.0828$.

Function γ that appear in G_ω formulation is also blended in the same way whereby the values for γ_1 and γ_2 are given as:

$$\gamma_1 = \frac{\beta_1}{\beta^*} - \frac{\kappa^2}{\sigma_{w,1}\sqrt{\beta^*}} \quad (10)$$

$$\gamma_2 = \frac{\beta_2}{\beta^*} - \frac{\kappa^2}{\sigma_{w,2}\sqrt{\beta^*}} \quad (11)$$

Blending function F_1 is designed to be 1 in wall affected region and 0 away from the walls and is given by:

$$F_1 = \tanh(\Phi_1^4) \quad (12)$$

$$\Phi_1 = \min \left[\max \left(\frac{\sqrt{k}}{0.09\omega y}, \frac{500\mu}{\rho y^2 \omega} \right), \frac{4\rho k}{\sigma_{\omega,2} D_\omega^+ y^2} \right] \quad (13)$$

$$D_\omega^+ = \max \left[2\rho \frac{1}{\sigma_{\omega,2}} \frac{1}{\omega} \frac{\partial k}{\partial x_j} \frac{\partial \omega}{\partial x_j}, 10^{-20} \right] \quad (14)$$

where y is the distance to the next surface and D_ω^+ is the positive portion of the cross-diffusion term (see below).

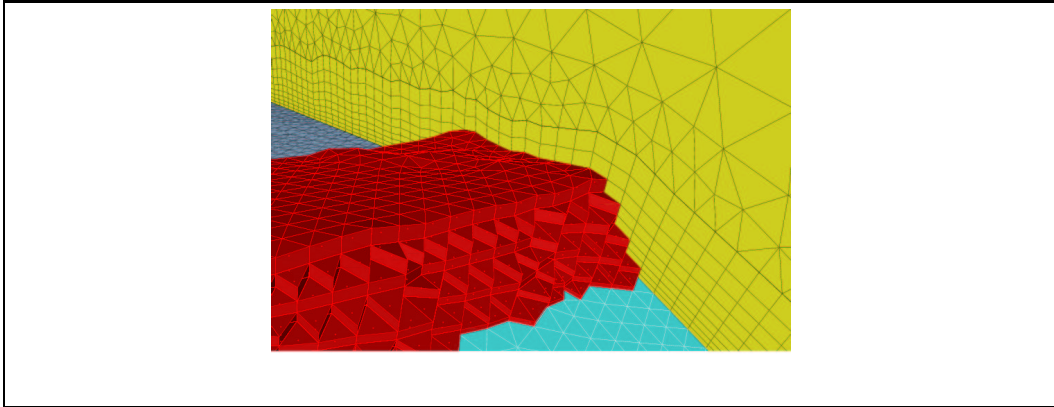


Figure 1: Grid in the boundary layer near the slant edge of the 25° Ahmed body

3.2.1 Turbulent Viscosity

Turbulent viscosity, μ_t , is computed as follows:

$$\mu_t = \frac{\rho k}{\omega} \frac{1}{\max \left[1, \frac{\Omega F_2}{a_1 \omega} \right]} \quad (15)$$

where $\Omega \equiv \sqrt{2\Omega_{ij}\Omega_{ij}}$, $a_1 = 0.31$ and Ω_{ij} is the mean rate-of-rotation tensor. The blending function F_2 is defined as:

$$F_2 = \tanh(\Phi_2^2) \quad (16)$$

$$\Phi_2 = \max \left[2 \frac{\sqrt{k}}{0.09 \omega y}, \frac{500 \mu}{\rho y^2 \omega} \right] \quad (17)$$

4 Computational Grid and Boundary Conditions

The grid has been generated using FLUENT's preprocessor GAMBIT. An unstructured grid consisting of about 2.3 million cells has been made for the half body. The boundary layer has been resolved using 9 layers of prisms (see Figure 1), while the rest of the grid consists of tetrahedral cells.

As boundary conditions for the flow and the turbulence equations the profiles provided by the workshop organizers has been used.

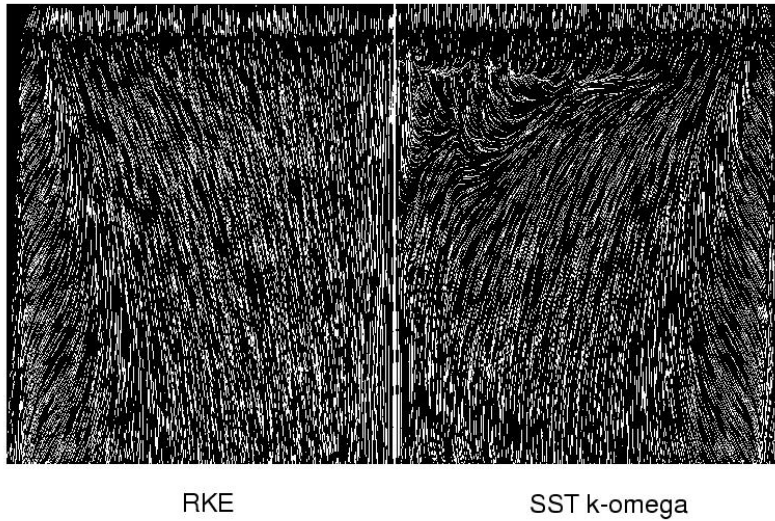


Figure 2: Oil flow on the slant of the Ahmed body 25°

5 Results

All results refer to computations performed for a slant angle of 25° , since this angle shows some interesting characteristics. As can be seen from the experiments from Lienhart [2] the flow shows some separation already at this slant angle. This behavior wasn't captured by the RKE while the SST $k-\omega$ seems to predict the existence of a separation bubble, see Figure 2.

The recirculation does not show up in local velocity profiles due to interpolation of data, see Figures 3. The recirculation bubbles spans only one cell layer. Using a refined grid might give a better resolution of this flow feature. Comparing the local profiles against experimental data give pretty good results on the top of the Ahmed body for both turbulence models. Along the slant both turbulence models show similar behavior. Their comparison with experimental data show a good qualitative agreement.

The distribution of turbulent kinetic energy is shown for RKE and SST $k-\omega$ in several planes behind the Ahmed body, see Figures 4, 5, and on the symmetry plane, see Figure 6. They look similar to experimental results.

Ahmed [1] provides experimental data of the local drag for the different parts of the vehicle. The results for two chosen turbulence models are given in Figure 7. While both turbulence models give a good prediction of the overall drag, there are differences to experimental results in the local drag.

9th ERCOFTAC/IAHR Workshop on Refined Turbulence Modelling
"Simulation of the Ahmed Body"

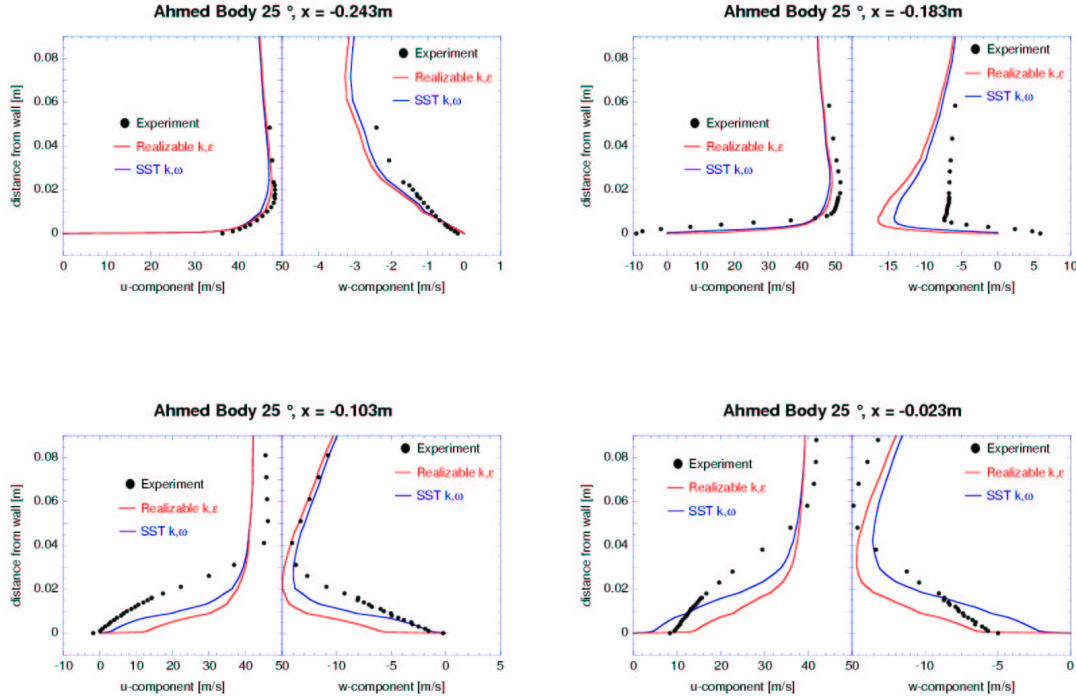


Figure 3: Local u, w velocity profiles in front of ($x=-0.243$) and on the slant of Ahmed body 25°

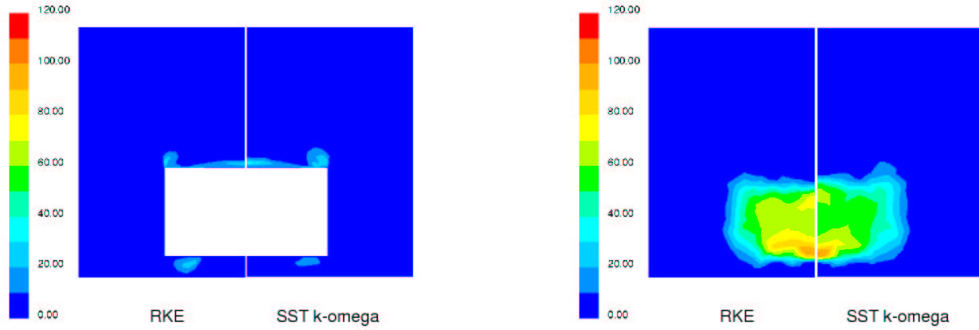


Figure 4: Turbulent kinetic energy behind the Ahmed body 25° : left $x = -0.0038m$, right $x = 0.08m$

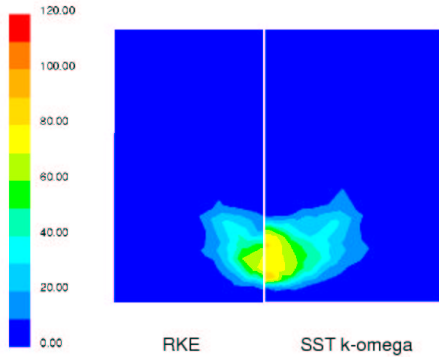


Figure 5: Turbulent kinetic energy behind the Ahmed body 25° , $x = 0.2m$

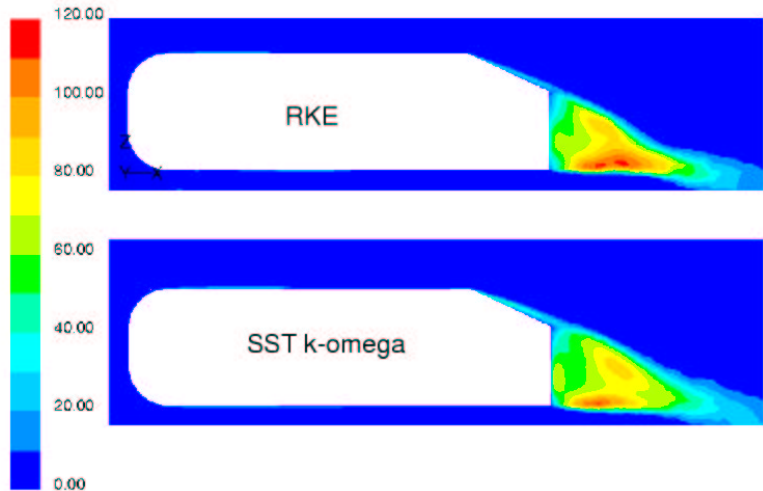


Figure 6: Turbulent kinetic energy in symmetry plane of the Ahmed body 25°

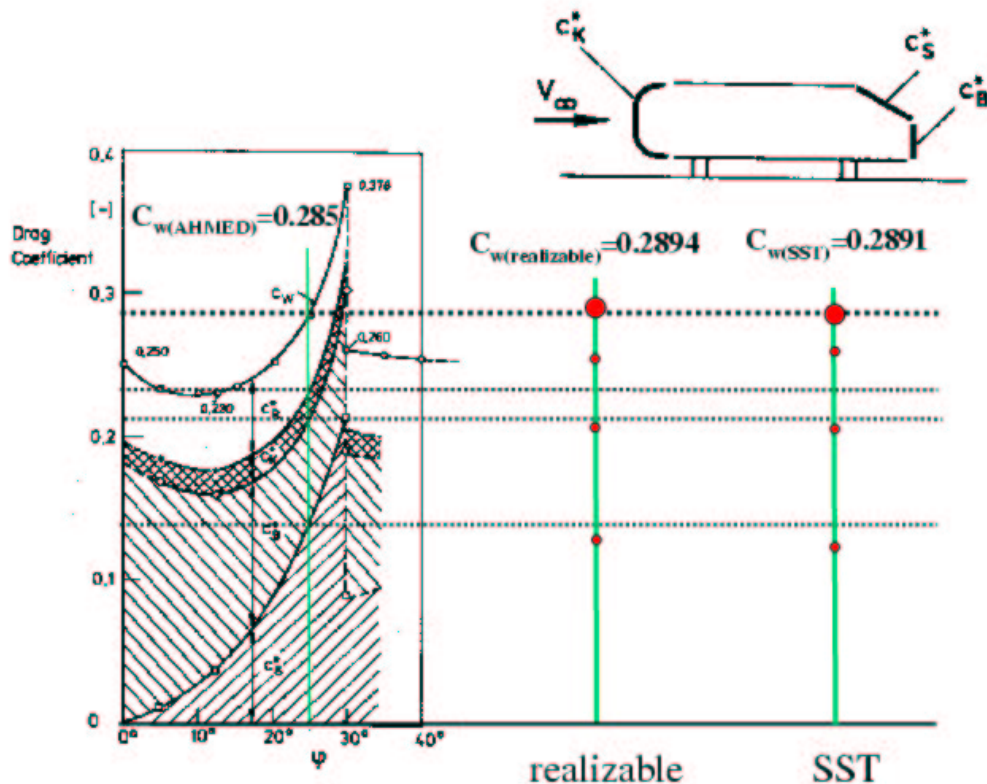


Figure 7: Local drag coefficient for two RANS turbulence models

6 Conclusion

The computation of the Ahmed body gave good qualitative and quantitative prediction of the three-dimensional flow around a bluff body for the realizable $k-\epsilon$ and the SST- $k-\omega$ turbulence model. The latter could capture a small recirculation bubble behind the slant edge. This needs to be investigated further using a refined grid. The overall drag showed a good agreement with experimental data, while distribution of the drag components of the different parts of the Ahmed body requires some further investigation.

References

- [1] G. Ramm S. Ahmed and G. Faltin. Some salient features of the time-averaged ground vehicle wake. *SAE Paper 840300*, 1984.
- [2] Lienhart Becker and Stoots. Flow and turbulence structures in the wake of a simplified car model (ahmed model). *DGLR Fach Symposium der AG STAB Stuttgart University, 15.-17. November, 2000*.
- [3] S.R. Mathur and J.Y. Murthy. A pressure-based method for unstructured meshes. *Numerical Heat Transfer*, 31:195–215, 1997.
- [4] A. Shabbir T.-H. Shih, W. W. Liou and J. Zhu. A new $k-\epsilon$ eddy-viscosity model for high reynolds number turbulent flows. *Computers Fluids*, 24(3):227–238, 1995.
- [5] F. Menter. Two-equation eddy-viscosity turbulence models for engineering applications. *AIAA Journal*, 32:1598–1605, 1994.

Case 9.4: (Ahmed body)

Flow around a simplified car body

LES with wall functions

C.Hinterberger, W. Rodi
Institut für Hydromechanik, Universität Karlsruhe
Kaiserstraße 12, 76128, Germany
hinterberger@ifh.uni-karlsruhe.de

Method

- LESOCC2-Code (Large Eddy Simulation on Curvilinear Coordinates)
- Finite-Volume, Hexaedra, structured, body fitted multi block grid
- Collocated arrangement, Rhie and Chow momentum interpolation
- SIMPLE method for velocity pressure coupling
- Pressure correction equation solved with SIP
- Runge-Kutta time stepping, pressure equation is solved only in last substep, second order
- Fluxes (convective and diffusive) discretized with second order central differences
- Parallelization by domain decomposition using MPI

Parameters

- Flow parameters:

Experiment: $U_b = 40[m/s]$, $L = 1.044[m]$, $Re = U \cdot L / \nu = 2784000$

Simulation: $U_b^* = 1$, $L^* = 1.044$, $1/\nu^* = Re/(U_b^* \cdot L^*)$

- Size of computational domain: $[-2.344, 5] \times [-0.935, 0.935] \times [0, 1.4]$
- Grid: 93 blocks, $8.8 \cdot 10^6$ cells
- Subgrid scale model: Smagorinsky model, $C_S = 0.13$
- Boundary conditions:

Inflow boundary at $x = -2.344[m]$, $U_b = 40[m/s]$ with superimposed random fluctuations (Gaussian white noise) $u'_{rms} = 0.36[m/s]$, $v'_{rms} = 0.2[m/s]$, $w'_{rms} = 0.2[m/s]$

Convective outflow boundary at $x = 5[m]$

Logarithmic law of the wall is applied at the walls of the ahmed body and at the bottom of the channel

Slip boundaries at the top and the sides of the channel

- Adaptive time stepping with maximum Courant number = 0.66, $\Delta t^* \approx 4.5 \cdot 10^{-4}$ ($\Delta t \approx 1.25 \cdot 10^{-5}[s]$)

- Averaging time: $T^* \approx 8.5$ ($T \approx 0.21[s]$)
- Simulations were performed using up to 30 processors on the IBM SP-SMP of the University Computing Center Karlsruhe. Each at a cost of approximately 5000 CPU hours.

Grid

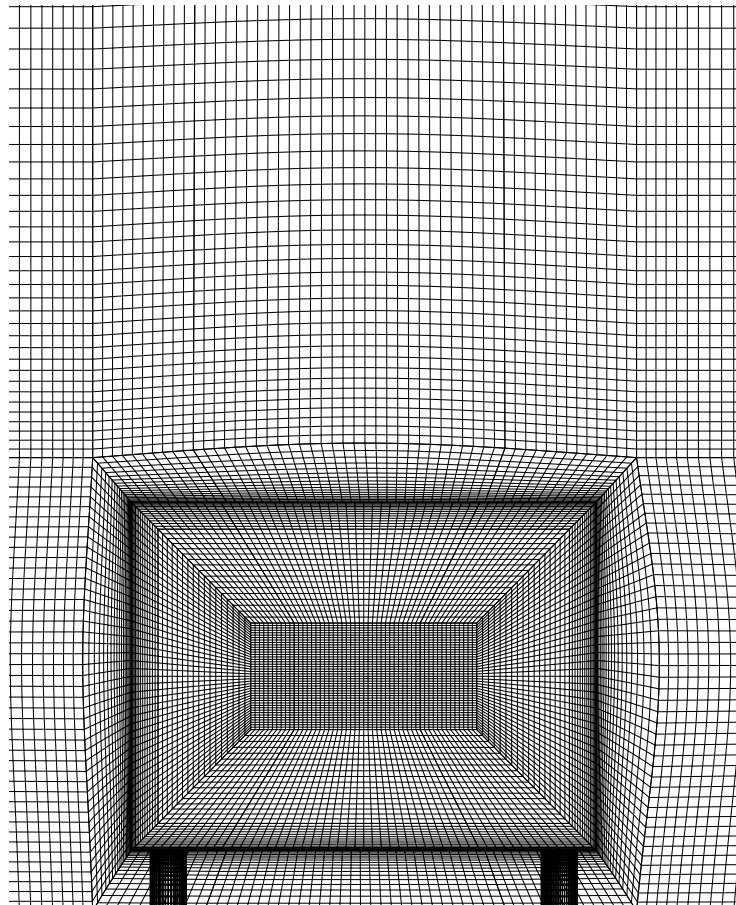


Figure 1: Cut in $y - z$ direction through a typical grid used for the simulation.

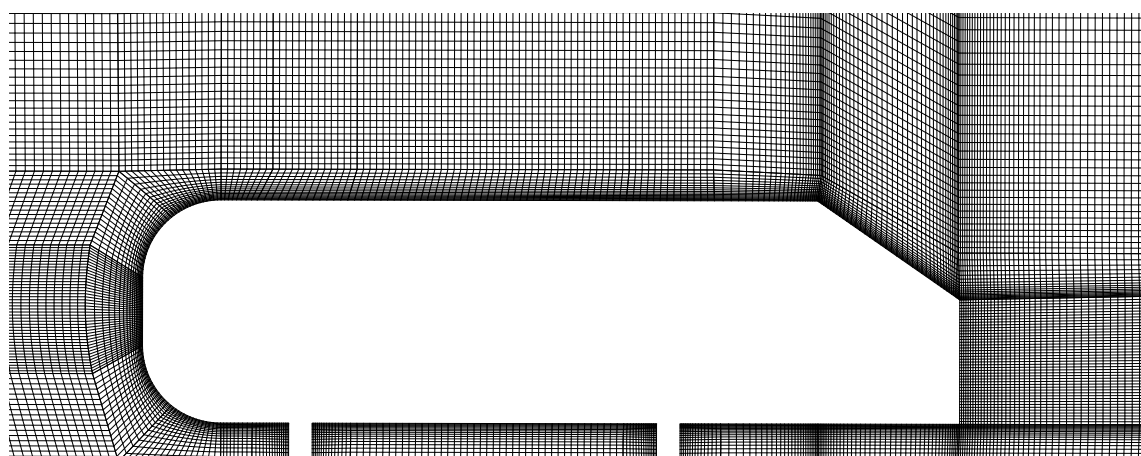


Figure 2: Cut in $x - z$ direction through the grid. (35° slant angle)

9th ERCOFTAC/IAHR Workshop on Refined Turbulence Modelling
Darmstadt, Germany, October 4–5, 2001.

Test-case 9.4: Flow around a simplified car body

(Ahmed body)

Description of the Model and Computational Method

O. Ouhlous, W. Khier, Y. Liu and K. Hanjalić

*Faculty of Applied Sciences, Delft University of
Technology, Lorentzweg 1, 2628 CJ Delft, The Netherlands*

Flow description

Air flow around a typical road vehicle is essentially three dimensional with a high degree of unsteadiness and strong interaction between numerous areas of flow separation. As a result, any symmetric analysis of the flow physics may lead to misinterpretation of the real physics. This has resulted in the proposition of simplified, or basic, car shapes of reduced geometrical complexity. Those simplified shapes are specially designed for retraining only those flow phenomena under consideration so that their effect can be studied in detail. The same practice has been adopted in MOVA project (Models for Vehicle Aerodynamics project) and Ahmed car shape has been chosen as a benchmark test case for model evaluation and development activities. In our computations 500.000 control volumes distributed over 33 blocks were used to compute the flow around the 35° Ahmed body. Figure 1 shows

the computational domain. The flow domain extended one body length upstream, left, right and above the model while the outlet boundary was situated five body lengths downstream of the car. The computations reproduced the same ground conditions as the wind tunnel measurements performed by LSTM. The model was supported by four slits of 50 mm above a solid stationary ground 2. On the inflow, a uniform velocity profile of 40 m/s was imposed and turbulence intensity of 2.5 percent. Symmetry

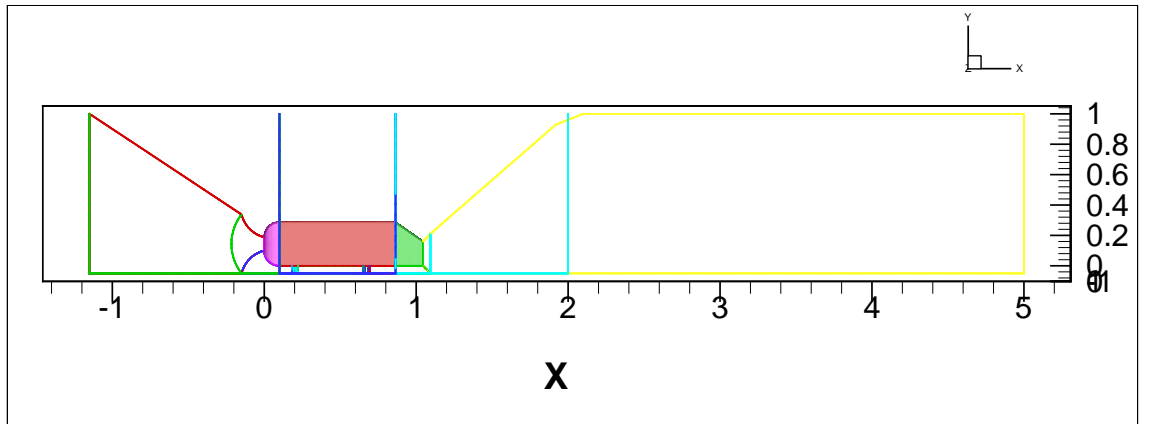


Figure 1: Dimension of Ahmed body

boundary conditions were imposed on the side and the top of boundaries and non slip condition on the surfaces of the model and the ground. All computations were performed on 16 processors of the TU-Delft CRAY T3E

Computation method and code description

The flow considered was computed with the X-STREAM finite-volume structured Navier-Stokes code. Cartesian vector and tensor components are used in colocated variable arrangement. The variables are defined in the cell centres, varying linearly in between. A pressure-correction method based on SIMPLE algorithm is used for pressure-velocity coupling. A hybrid descretization was employed for the convective and dissipative terms. The computations were advanced in time at intervals of 10^{-3} seconds to satify the CFL condition. The code uses the three-level time-integration scheme, the computations were performed using a true-time marching.

Mesh used

The grid was generated using the commercial FLUENT grid generator GAMBIT. Using a grid converter the unstructured GAMBIT grid have been converted into a block structured grid. Figure 2 shows the grid points on the surface.

The mesh contains about 500.000 cells in a total of 33 blocks. The first y^+ on the body top surface is around 60

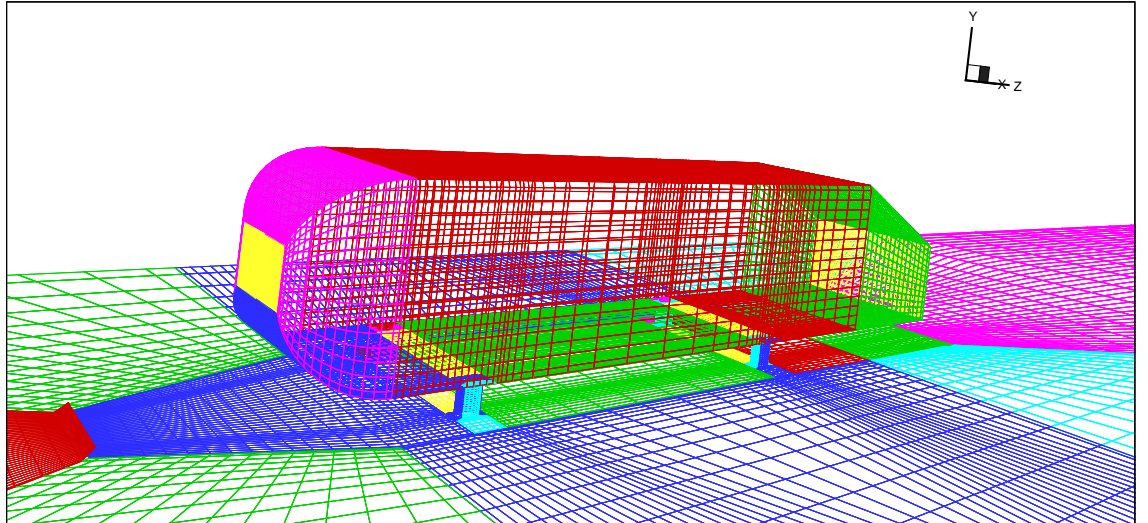


Figure 2: Figure 2: Geometry and surface grid

Turbulence model

The complexity of the flow around made it interesting to test several turbulence model on this test case. The simulation of the 35^0 Ahmed body were performed using:

- The standard $k - \varepsilon$ model
- SSG Reynolds-stress model with standard wall function
- SSG Reynolds-stress model with new non-equilibrium wall function
- $k - \varepsilon - \overline{v^2}$ with wall function
- Elliptic Blending Reynolds-stress model EBM with wall function

References

- (1) Speziale, C.G., S. Sarkar, and T. B. Gatski (1991). Modelling the pressure-strain correlation of turbulence: an invariant dynamical systems approach. *J. fluid Mech.* 227, 245-272.
- (2) Manceau R. and K. Hanjalić, A new form of the elliptic relaxation equation to account for wall effects in RANS modelling.
- (3) Durbin P.A., (1991): *Near-Wall Turbulence Closure Modeling Without*

"Damping Functions", Theoretical and Computational Fluid Dynamics, Vol. 3, 1–13.

Figures

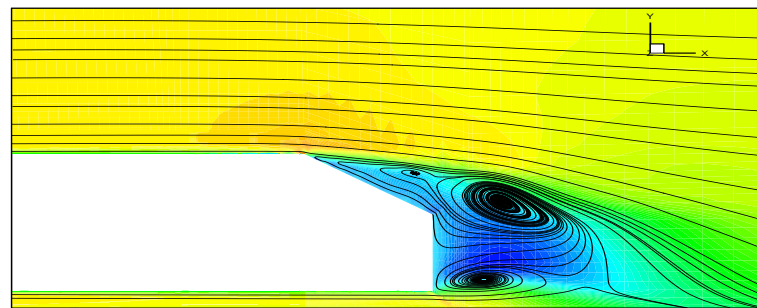


Figure 3: Streamlines in the wake of Ahmed body (St. SSG model)

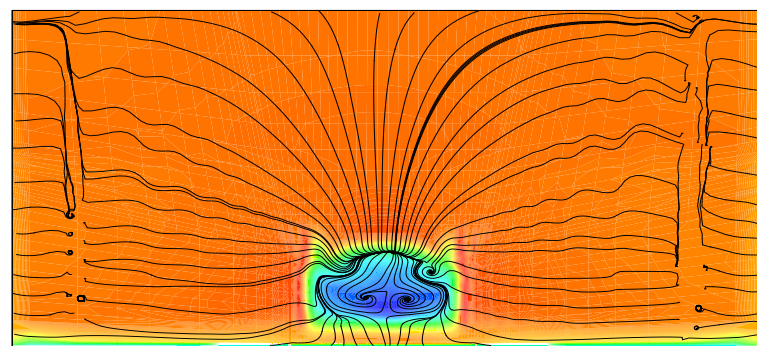


Figure 4: $x = 277\text{mm}$

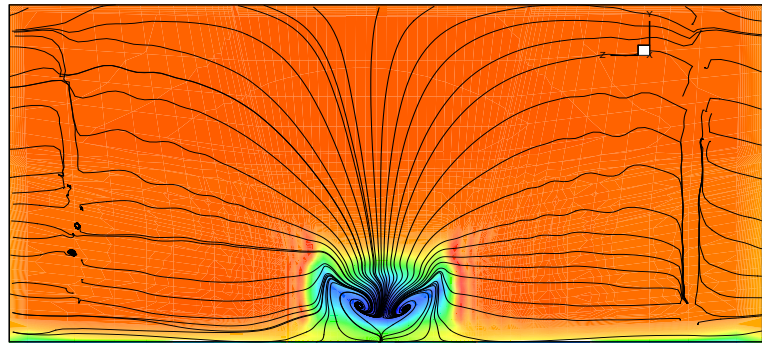


Figure 5: $x = 694\text{mm}$

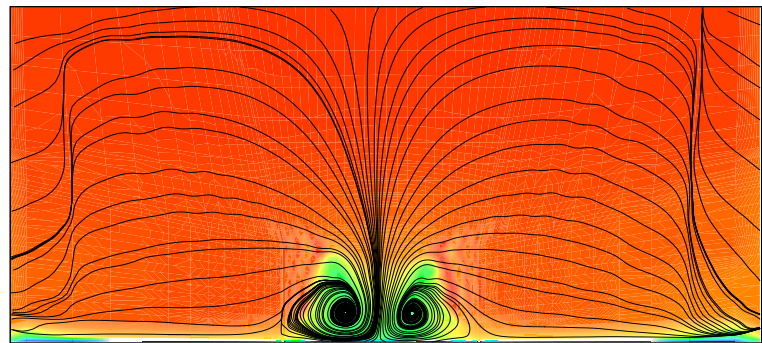


Figure 6: $x = 1736\text{mm}$

Figure 7: Streamlines in the wake of Ahmed body. Form top to bottom:
 $x/L=0.277, 0.694, 1.736$. Calculated by the St. SSG model

COMPUTATIONAL STUDY OF FLOW AROUND THE “AHMED” CAR BODY (CASE 9.4)

T. J. Craft, S. E. Gant, H. Iacovides, B. E. Launder and C. M. E. Robinson

Department of Mechanical, Aerospace and Manufacturing Engineering,
University of Manchester Institute of Science and Technology (UMIST),
PO Box 88, Manchester, M60 1QD, UK
web page: <http://cfd.me.umist.ac.uk/>

A number of RANS simulations of flow around the “Ahmed” body have been undertaken for the 9th ERCOFTAC/IAHR Workshop on Refined Turbulence Modelling. These calculations form part of a more detailed study of vehicle aerodynamics supported by European Union BRITE/EURAM Models for Vehicle Aerodynamics (MOVA) project (BE-97-4043). The simulations have involved two different turbulence models: a linear and a non-linear $k - \varepsilon$ model, and two different wall functions.

1 Numerical Methods

The flow around the Ahmed body was studied using the STREAM CFD code of Lien of Leschziner [5] (Simulation of Turbulent Reynolds-averaged Equations for All Mach numbers). STREAM is a three-dimensional, fully-elliptic, finite-volume solver which uses a structured, non-orthogonal, curvilinear, multi-block grid and a fully-collocated arrangement for data storage. The code uses the SIMPLE pressure-correction algorithm [8] and a Rhie & Chow interpolation [9] to prevent unrealistic pressure fluctuations due to the non-staggered grid arrangement. Convection is discretized using either an upwind scheme or UMIST (Upstream Monotonic Interpolation for Scalar Transport) a TVD scheme based on the third-order accurate QUICK [6]. In the majority of the Ahmed body computations, the UMIST scheme was used for convection of both momentum and turbulence scalars, but in some cases it was necessary to use the less accurate but more stable upwind scheme (see Table 1). This was due, firstly, to the Analytical Wall Function (AWF) which could not be implemented as robustly as the standard log-law Simplified Chieng & Launder (SCL) wall function and, secondly, to the grid which contained some skewed cells with corner angles of approximately 45° . Calculations were converged until velocity, mass and turbulence residuals were below 10^{-4} . A number of tests were undertaken in order to ensure that the results obtained were fully converged, including running some time-dependent calculations, for details see Robinson [10].

2 Computational Grids

Separate computational grids were defined for the 25° and 35° Ahmed bodies which principally differed over the rear slant, although there were minor differences in the grid structure over the upstream portion of the body (see Figures 1, 2 and 3). Both grids used 22 blocks and approximately

Rear Slant	Model	Wall Function	Mean Velocities	Turb. Variables
25°	Linear	SCL	UMIST	UMIST
		AWF	UMIST	UMIST
	Non-Linear	SCL	UMIST	UMIST
		AWF	UMIST	Upwind
35°	Linear	SCL	UMIST	UMIST
		AWF	UMIST	Upwind
	Non-Linear	SCL	UMIST	Upwind
		AWF	UMIST	Upwind

Table 1: Convection schemes used in calculations of Ahmed body flow

300,000 cells, as shown in Table 2. The legs, or stilts, on which the model is supported in the wind tunnel experiments, were not included in the computational grid. Grids were adjusted to maintain y^* values of as many as possible near-wall cells around the body to within the limits $55 < y^* < 550$, but these limits were exceeded in regions of stagnation, separated and reattachment. The y^* values of the near-wall cells adjacent to the ground plane were not controlled, as to maintain $y^* < 550$ required high-aspect ratio cells which compromised the stability of the calculation. Due to the large number of nodes required to model the Ahmed body, it was not possible to refine the grids and establish grid independence. However, a coarser grid was generated for the 25° Ahmed body to investigate the effect of grid coarsening and provide some information regarding grid independence (see [10]).

Slant Angle	No. Blocks	No. Cells
25°	22	331,000
35°	22	355,000

Table 2: Ahmed body grids with the number of cells to the nearest thousand

3 Boundary Conditions

The floor of the domain and the Ahmed body itself were treated as wall boundary conditions, using either the Simplified Chieng & Launder (SCL) wall function or the Analytical Wall Function (AWF) (see Figure 4). The centreline of the body (at $y = 0$), the opposite boundary at the outside limit of the domain ($y = 1.044\text{m}$) and the upper domain boundary ($z = 1.044\text{m}$) were all treated as symmetry planes. Ideally the latter two would be treated as entrainment boundaries. Symmetry planes were used instead to provide a more stable calculation and were justifiable as there is little deflection of the flow at these boundaries. The downstream outlet was set with zero-gradient for all variables. LSTM provided measurements of the streamwise velocity and Reynolds stress upstream of the body ($x = -1.444\text{m}$). These profiles were used to define the inlet velocity and turbulence profiles to the calculation. However, the velocity profiles showed that at $x = -1.444\text{m}$ there was a deflection of the flow due to the blockage effect of the body which resulted in a lower mean U -velocity (38.51ms^{-1}) approaching the body across the height of the domain than the experimental bulk U -velocity (40.0ms^{-1}). Consequently, the inlet profiles were scaled to achieve agreement with the experimental velocity profiles upstream of the body, which gave an inlet

Reynolds number $Re = 7.57 \times 10^5$ (based on the body's height and inlet bulk velocity). The Reynolds number is sufficiently high that this minor adjustment should not have significantly influenced the results. At the inlet, flat profiles of turbulent kinetic energy, k_{in} , and dissipation rate, ε_{in} , were specified: $k_{in} = 7.10 \times 10^{-3}$ and ε_{in} was calculated from an assumed ratio of the turbulent to the molecular viscosity, $\nu_t/\nu = 60$. At a later date, LSTM provided a more accurate estimate of the experimental inlet dissipation rate ($\nu_t/\nu \approx 10$). Tests showed that switching to the new value had no impact on the calculated flow around the body.

4 Turbulence Models

Two turbulence models were used to calculate the flow around the Ahmed body: the linear $k - \varepsilon$ model of Launder & Spalding [4] and the non-linear $k - \varepsilon$ model of Craft *et al.* [3]. The linear $k - \varepsilon$ model used a realizability constraint to avoid excessively large values of μ_t in regions of low turbulence and inviscid deflection of the flow. This viscosity limiter was not used with the non-linear model, which incorporates a functional form of c_μ that reduces μ_t in regions where the strain and vorticity invariants (S and Ω) are high.

Linear $k - \varepsilon$ Model

In the high-Reynolds-number form of the $k - \varepsilon$ model by Launder & Spalding [4], the Reynolds stress, $\overline{u_i u_j}$ is a linear function of the strain-rate, and the eddy-viscosity is calculated from the turbulent kinetic energy, k , and dissipation rate, ε , as follows:

$$\nu_t = c_\mu \frac{k^2}{\varepsilon} \quad (1)$$

Transport equations are solved for k and ε , which for a steady flow can be expressed in Cartesian tensors as follows:

$$\frac{\partial(\rho U_j k)}{\partial x_j} = \frac{\partial}{\partial x_j} \left[\left(\mu + \frac{\mu_t}{\sigma_k} \right) \frac{\partial k}{\partial x_j} \right] + P_k - \rho \varepsilon \quad (2)$$

$$\frac{\partial(\rho U_j \varepsilon)}{\partial x_j} = \frac{\partial}{\partial x_j} \left[\left(\mu + \frac{\mu_t}{\sigma_\varepsilon} \right) \frac{\partial \varepsilon}{\partial x_j} \right] + c_{\varepsilon 1} f_1 P_k \frac{\varepsilon}{k} - c_{\varepsilon 2} f_2 \rho \frac{\varepsilon^2}{k} \quad (3)$$

A realizability constraint derived by May [7] was used in conjunction with the linear $k - \varepsilon$ model and was coded into STREAM as follows:

$$\mu_t = \min \left[\mu_t, \frac{\rho k}{\max(TINY, \alpha_1, \alpha_2, \alpha_3)} \right] \quad (4)$$

where $TINY$ is an arbitrarily small value and α_1 , α_2 and α_3 are given by:

$$\alpha_1 = \frac{3}{2} \left\{ \frac{\partial U}{\partial x} + \frac{\partial V}{\partial y} + \left[\left(\frac{\partial V}{\partial y} - \frac{\partial U}{\partial x} \right)^2 + \left(\frac{\partial U}{\partial y} - \frac{\partial V}{\partial x} \right)^2 \right]^{1/2} \right\} \quad (5)$$

$$\alpha_2 = \frac{3}{2} \left\{ \frac{\partial V}{\partial y} + \frac{\partial W}{\partial z} + \left[\left(\frac{\partial W}{\partial z} - \frac{\partial V}{\partial y} \right)^2 + \left(\frac{\partial V}{\partial z} - \frac{\partial W}{\partial y} \right)^2 \right]^{1/2} \right\} \quad (6)$$

$$\alpha_1 = \frac{3}{2} \left\{ \frac{\partial W}{\partial z} + \frac{\partial U}{\partial x} + \left[\left(\frac{\partial U}{\partial x} - \frac{\partial W}{\partial z} \right)^2 + \left(\frac{\partial W}{\partial x} - \frac{\partial U}{\partial z} \right)^2 \right]^{1/2} \right\} \quad (7)$$

In a simple shear flow the latter part of the minimum function in Equation (4) can be rearranged to express c_μ as a function of the strain invariant, S :

$$c_\mu = \frac{2}{3S} \quad (8)$$

Non-Linear $k - \varepsilon$ Model

In the non-linear $k - \varepsilon$ model of Craft *et al.* [3], additional quadratic and cubic functions of strain and vorticity are introduced into the equation for the Reynolds stress, as follows:

$$\begin{aligned} -\overline{u_i u_j} + \frac{2}{3} \delta_{ij} k = & \nu_t S_{ij} \\ & + c_1 \frac{\nu_t k}{\varepsilon} (S_{ik} S_{kj} - \frac{1}{3} S_{kl} S_{kl} \delta_{ij}) \\ & + c_2 \frac{\nu_t k}{\varepsilon} (\Omega_{ik} S_{kj} + \Omega_{jk} S_{ki}) \\ & + c_3 \frac{\nu_t k}{\varepsilon} (\Omega_{ik} \Omega_{kj} - \frac{1}{3} \Omega_{lk} \Omega_{lk} \delta_{ij}) \\ & + c_4 \frac{\nu_t k^2}{\varepsilon^2} (S_{ki} \Omega_{lj} + S_{kj} \Omega_{li}) S_{kl} \\ & + c_5 \frac{\nu_t k^2}{\varepsilon^2} (\Omega_{il} \Omega_{lm} S_{mj} + S_{il} \Omega_{lm} \Omega_{mj} - \frac{2}{3} S_{lm} \Omega_{mn} \Omega_{nl} \delta_{ij}) \\ & + c_6 \frac{\nu_t k^2}{\varepsilon^2} S_{ij} S_{kl} S_{kl} \\ & + c_7 \frac{\nu_t k^2}{\varepsilon^2} S_{ij} \Omega_{kl} \Omega_{kl} \end{aligned} \quad (9)$$

This model also takes c_μ to be a function of the invariants of the strain and vorticity tensors:

$$c_\mu = \frac{0.3}{1 + 0.35 [\max(S, \Omega)]^{1.5}} (1 - \exp \{-0.36 \exp [0.75 \max(S, \Omega)]\}) \quad (10)$$

and the so-called “Yap correction”, Y_c , is included as a source term in the ε -equation. The standard Yap correction is based on the ratio of the length scale, $k^{3/2}/\varepsilon$, to the equilibrium length scale, defined by $l_e = 2.55y$, where y is the wall-normal distance:

$$Y_c = \max \left[0.83 \left(\frac{k^{3/2}/\varepsilon}{2.55y} - 1 \right) \left(\frac{k^{3/2}/\varepsilon}{2.55y} \right)^2, 0 \right] \quad (11)$$

5 Wall Functions

Two wall functions were used in the Ahmed body calculations: the log-law-based Simplified Chieng & Launder (SCL) wall function and a new Analytical Wall Function (AWF). These wall functions are similar in terms of implementation: both employ a no-slip condition at the wall surface ($U_i = 0$), the velocity variation within the near-wall cell is accounted for by setting to zero the momentum flux to the wall and including in its place an expression for the wall shear stress, τ_{wall} . Likewise, the production and dissipation source terms (P_k and ε) in the the discretized

k -equation within the near-wall cells are replaced with cell-averaged production and dissipation source terms ($\overline{P_k}$ and $\overline{\varepsilon}$). In both wall functions, the ε -equation is not solved in the near-wall cell and instead its value at the near-wall node is prescribed from assuming an equilibrium turbulence length scale variation, $k^{3/2}/\varepsilon = c_l y$.

Simplified Chieng & Launder (SCL)

The wall function proposed by Chieng & Launder [1] divided the near-wall cell divided into two layers: the viscous sublayer (defined as $y^* = yk^{1/2}/\nu < 20$) and the fully turbulent region. In the viscous sublayer the velocity was assumed to increase linearly, the shear stress to be zero and the turbulent kinetic energy to vary quadratically, whilst in the fully turbulent region the velocity was assumed to follow the “universal” log-law profile and both $\rho \overline{uv}$ and k were assumed to vary linearly with wall distance. Since at the wall the dissipation rate is given by $\varepsilon = 2\nu (\partial k^{1/2} / \partial y)^2$ and k varies quadratically, ε was assumed to take a constant value in the viscous sublayer. In the fully turbulent region, ε was obtained from assuming an equilibrium turbulence length scale variation, $k^{3/2}/\varepsilon = c_l y$ (where $c_l = 2.55$). The simplified version of the wall function employed in the Ahmed body calculations assumed a constant turbulent kinetic energy and shear stress in the fully turbulent region. This gave the following expression for the wall shear stress, τ_{wall} , average production, $\overline{P_k}$ and average dissipation $\overline{\varepsilon}$:

$$\begin{aligned}\tau_{wall} &= \frac{\rho \kappa c_\mu^{1/4} k_p^{1/2} U_p}{\ln \left(Ec_\mu^{1/4} k_p^{1/2} y_p / \nu \right)} \\ \overline{P_k} &= \frac{1}{y_n} \int_{y_v}^{y_n} \tau_{wall} \cdot \frac{\tau_{wall}}{\kappa c_\mu^{1/4} \rho k_p^{1/2} y} dy = \frac{\tau_{wall}^2}{\kappa c_\mu^{1/4} \rho k_p^{1/2} y_n} \ln \left(\frac{y_n}{y_v} \right) \\ \overline{\varepsilon} &= \frac{1}{y_n} \left(y_v \frac{2\nu k_p}{y_v^2} + \int_{y_v}^{y_n} \frac{c_\mu^{3/4} k_p^{3/2}}{\kappa y} dy \right) = \frac{1}{y_n} \left(\frac{2\nu k_p^{3/2}}{k_p^{1/2} y_v / \nu} + \frac{c_\mu^{3/4} k_p^{3/2}}{\kappa} \ln \left(\frac{y_n}{y_v} \right) \right)\end{aligned}$$

where subscript p denotes the value at the wall-adjacent node, U is the wall-parallel velocity and y_p the distance from the wall to the near-wall node and the sublayer thickness, y_v , is calculated from $y_v k_p^{1/2} / \nu = 20$.

Analytical Wall Function (AWF)

In the Analytical Wall Function (AWF) neither the log-law velocity profile nor the constant or linear variation in shear stress is assumed. Instead, a simplified momentum equation is specified in the near-wall cell:

$$\frac{\partial(\rho U U)}{\partial x} + \frac{\partial(\rho U V)}{\partial y} = -\frac{\partial p}{\partial x} + \frac{\partial}{\partial y} \left[(\mu + \mu_t) \frac{\partial U}{\partial y} \right] \quad (12)$$

and integrated analytically across the near-wall cell using a prescribed viscosity profile:

$$\begin{aligned}\mu_t &= 0 && \text{for } y < y_v \\ &= \rho c_\mu c_l k_p^{1/2} (y - y_v) && \text{for } y \geq y_v\end{aligned} \quad (13)$$

where $c_l = 2.55$. A detailed derivation of the analytical wall function can be found in Robinson [10] or in a similar approach for buoyancy-affected flows by Craft *et al.* [2]. Expressions for the wall shear stress and average production of turbulent kinetic energy for the near-wall cell are provided below:

$$\tau_w = -\frac{\rho k_p^{1/2}}{\mu_v} A_1$$

$$\overline{P}_k = \frac{\rho \alpha k_p^{1/2}}{y_n \mu_v} \int_{y_v^*}^{y_n^*} \mu_v (y^* - y_v^*) \left[\frac{A_1 + C_1 y_v^* + C_2 (y^* - y_v^*)}{\mu_v [1 + \alpha (y^* - y_v^*)]} \right]^2 dy^*$$

$$\bar{\varepsilon} = \frac{1}{y_n} \left[\frac{2k_p^{3/2}}{y_\varepsilon^*} + \frac{k_p^{3/2}}{c_l} \ln \left(\frac{y_n}{y_\varepsilon^*} \right) \right]$$

where constants A_1 , C_1 and C_2 are given by:

$$A_1 = \frac{\alpha \mu_v U_n - C_2 (y_n^* - y_v^*) + [C_1 y_v^* - \frac{C_2}{\alpha}] \ln [1 + \alpha (y_n^* - y_v^*)] + \frac{\alpha C_1 y_v^{*2}}{2}}{\alpha y_v^* + \ln [1 + \alpha (y_n^* - y_v^*)]}$$

$$C_1 = \frac{\mu_v^2}{\rho^2 k_p} \left[\frac{\partial p}{\partial x} + \gamma \rho U \frac{\partial U}{\partial x} + \gamma \rho V \frac{\partial U}{\partial y} \right]$$

$$C_2 = \frac{\mu_v^2}{\rho^2 k_p} \left[\frac{\partial p}{\partial x} + \rho U \frac{\partial U}{\partial x} + \rho V \frac{\partial U}{\partial y} \right]$$

γ is an empirical constant which is used to control the influence of convection inside the laminar sub-layer, $\alpha = c_\mu c_l$. The turbulence and dissipation viscous sublayer thicknesses y_v^* and y_ε^* are 10.8 and 5.1 respectively.

6 Results Summary

A selection of results have been provided to show the main differences in the behaviour of the two turbulence models with different wall functions. For the 25° case, the LSTM experiments showed a small separation bubble at the leading edge of the rear slant, after which the boundary layer re-attached. The linear $k-\varepsilon$ model predicted attached flow over the whole of the slant whilst the non-linear model predicted fully separated flow (as shown in Figures 5 and 6). The development of attached or separated flow over the rear slant is strongly influenced by the presence of side-edge vortices which draw fluid out of the boundary layer on the rear slant. The weaker, more defined vortices predicted by the non-linear model led to the separation of the boundary layer. The velocity field was reasonably predicted by the linear $k-\varepsilon$ model over the 25° Ahmed body (Figure 6) but the predicted streamwise normal stress (\overline{uu}) was an order-of-magnitude lower than the experimental values (Figure 7). This discrepancy may have been due to some unsteadiness in the experimental flow, perhaps involving periodic separation, which was not resolved by the time-averaged measurements. The analytical wall function had little effect on the flow profiles shown in Figures 6 and 7, although it slightly improved in the overall drag predictions (see Table 3).

For the 35° Ahmed body, both linear and non-linear models correctly predicted separated flow over the rear slant. The linear $k-\varepsilon$ model gave reasonable predictions for the wake dimensions and velocity, although the predicted turbulent kinetic energy was too high (see Figure 12). The

Case	Pressure Coefficient			Skin Friction	Total Drag		%Error
	Nose	Slant	Base		No Stilt	With Stilt	
Ahmed <i>et al.</i> (1984)	0.020	0.140	0.070	0.055	-	0.285	-
LSTM	-	0.158	0.116	-	-	-	-
linear $k - \varepsilon$, SCL	0.048	0.139	0.103	0.004	0.294	0.311	9.1
linear $k - \varepsilon$, AWF	0.049	0.139	0.100	0.005	0.293	0.310	8.8
non-linear $k - \varepsilon$, SCL	0.047	0.105	0.111	0.004	0.267	0.286	0.4
non-linear $k - \varepsilon$, AWF	0.051	0.083	0.114	0.004	0.251	0.270	-5.3

Table 3: Drag predictions and experimental measurements for the 25° Ahmed body.

Case	Pressure Coefficient			Skin Friction	Total Drag		% Error
	Nose	Slant	Base		No Stilt	With Stilt	
Ahmed <i>et al.</i> (1984)	0.020	0.095	0.090	0.055	-	0.260	-
LSTM	-	0.121	0.129	-	-	-	-
linear $k - \varepsilon$, SCL	0.046	0.134	0.102	0.004	0.287	0.305	17.3
linear $k - \varepsilon$, AWF	0.047	0.112	0.103	0.005	0.267	0.286	10.0
non-linear $k - \varepsilon$, SCL	0.047	0.088	0.093	0.004	0.231	0.251	-3.1
non-linear $k - \varepsilon$, AWF	0.052	0.088	0.099	0.004	0.235	0.255	-1.5

Table 4: Drag predictions and experimental measurements for the 35° Ahmed body.

wake predicted by the non-linear $k-\varepsilon$ model (Figure 13) was both too high (in the z -axis) and too long (in the x -axis). The relatively poor prediction of the wake size with the non-linear model is in agreement with an earlier study of the flow over a square cylinder (Robinson, [10]). Streamwise velocity and Reynolds stress predictions were similar using either the simplified Chieng & Launder or the analytical wall functions (the non-linear model with AWF has not been displayed in Figures 10 and 11 as this result was practically identical to that obtained with SCL). However, drag predictions improved with the AWF and the combination of the non-linear model and the analytical wall function led to drag predictions within 2% of the experimental value (see Table 4).

Low-Reynolds-number model computations of the flow around the Ahmed body are in progress and will be reported at a later date.

References

- [1] C. C. Chieng and B. E. Launder. On the calculation of turbulent heat transport downstream from an abrupt pipe expansion. *Numerical Heat Transfer*, 3:189–207, 1980.
- [2] T. J. Craft, A. V. Gerasimov, H. Iacovides, and B. E. Launder. Progress in the generalization of wall-function treatments. In *Turbulent Heat Transfer III*, Alaska, 2001.
- [3] T. J. Craft, B. E. Launder, and K. Suga. Development and application of a cubic eddy-viscosity model of turbulence. *Int. J. Heat and Fluid Flow*, 17:108–115, 1996.
- [4] B. E. Launder and D. B. Spalding. The numerical computation of turbulent flows. *Computer Methods in Applied Mechanics and Engineering*, 3:269–289, 1974.

- [5] F. S. Lien and M. A. Leschziner. A general non-orthogonal finite-volume algorithm for turbulent flow at all speeds incorporating second-moment turbulence-transport closure. *Comp. Meth. Appl. Mech. Eng.*, 114:123–167, 1994.
- [6] F. S. Lien and M. A. Leschziner. Upstream monotonic interpolation for scalar transport with application to complex turbulent flows. *Int. J. Num. Meth. Fluids*, 19:527–548, 1994.
- [7] N. E. May. Efficient implementation of two-equation and differential Reynolds stress turbulence models into a cell-vertex, explicit, time-marching, Navier-Stokes flow code. Technical Report M345/1, Aircraft Research Assoc., 1998.
- [8] S. V. Patankar and D. B. Spalding. A calculation procedure for heat, mass and momentum transfer in three-dimensional parabolic flows. *Int. J. Heat Mass Transfer*, 15:1787, 1972.
- [9] C. M. Rhie and W. L. Chow. Numerical study of the turbulent flow past an airfoil with trailing edge separation. *AIAA J.*, 21:1525–1532, 1983.
- [10] C. M. E. Robinson. *Advanced CFD modelling of road-vehicle aerodynamics*. PhD thesis, Dept. of Mechanical Engineering, UMIST, 2001.

Figures

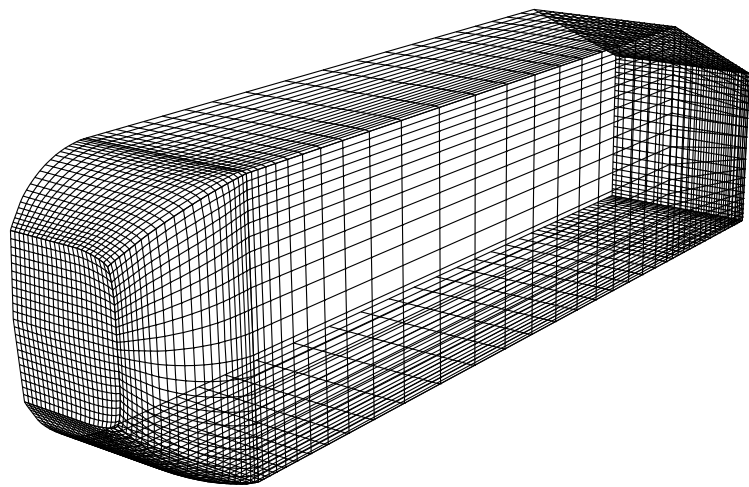


Figure 1: Grid on nose cone and front portion of Ahmed body

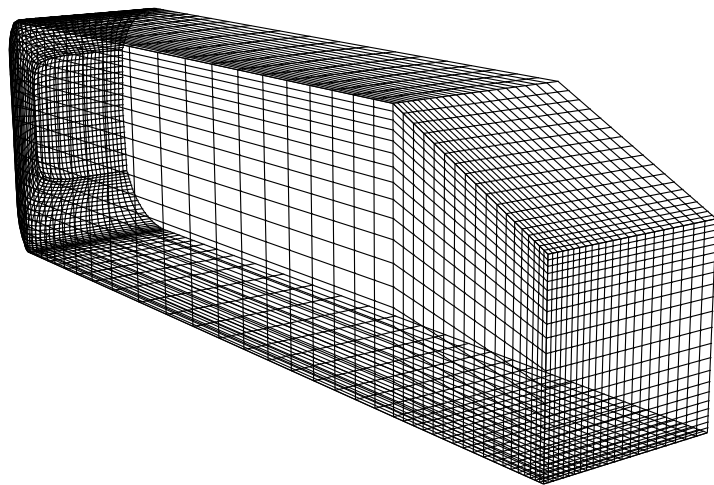


Figure 2: Grid used on rear section and slant of 25° Ahmed body

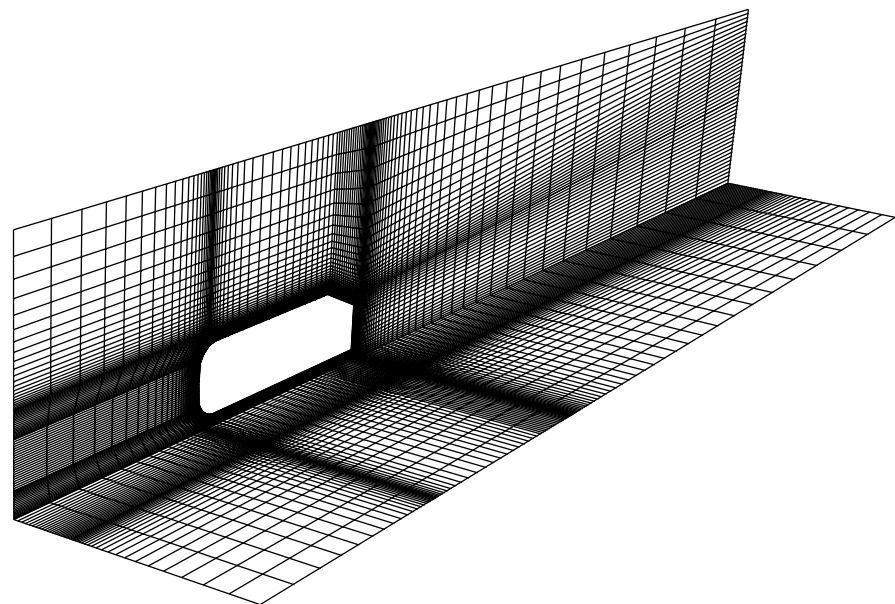


Figure 3: Grid on symmetry plane and floor showing some refinement propagated at block boundaries

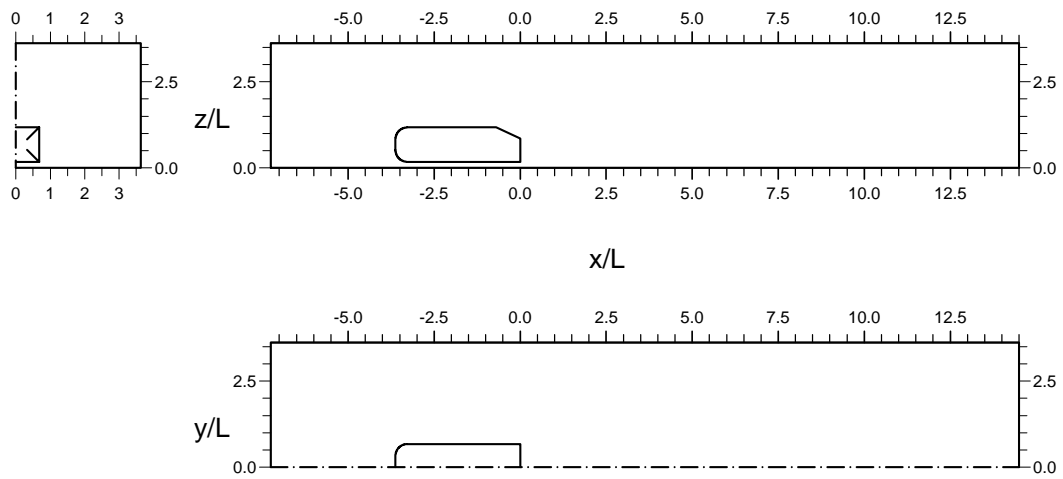


Figure 4: Sketch of domain in third angle projection used for Ahmed body calculations (lengths are non-dimensionalized with $L = 0.288\text{m}$, the height of the body)

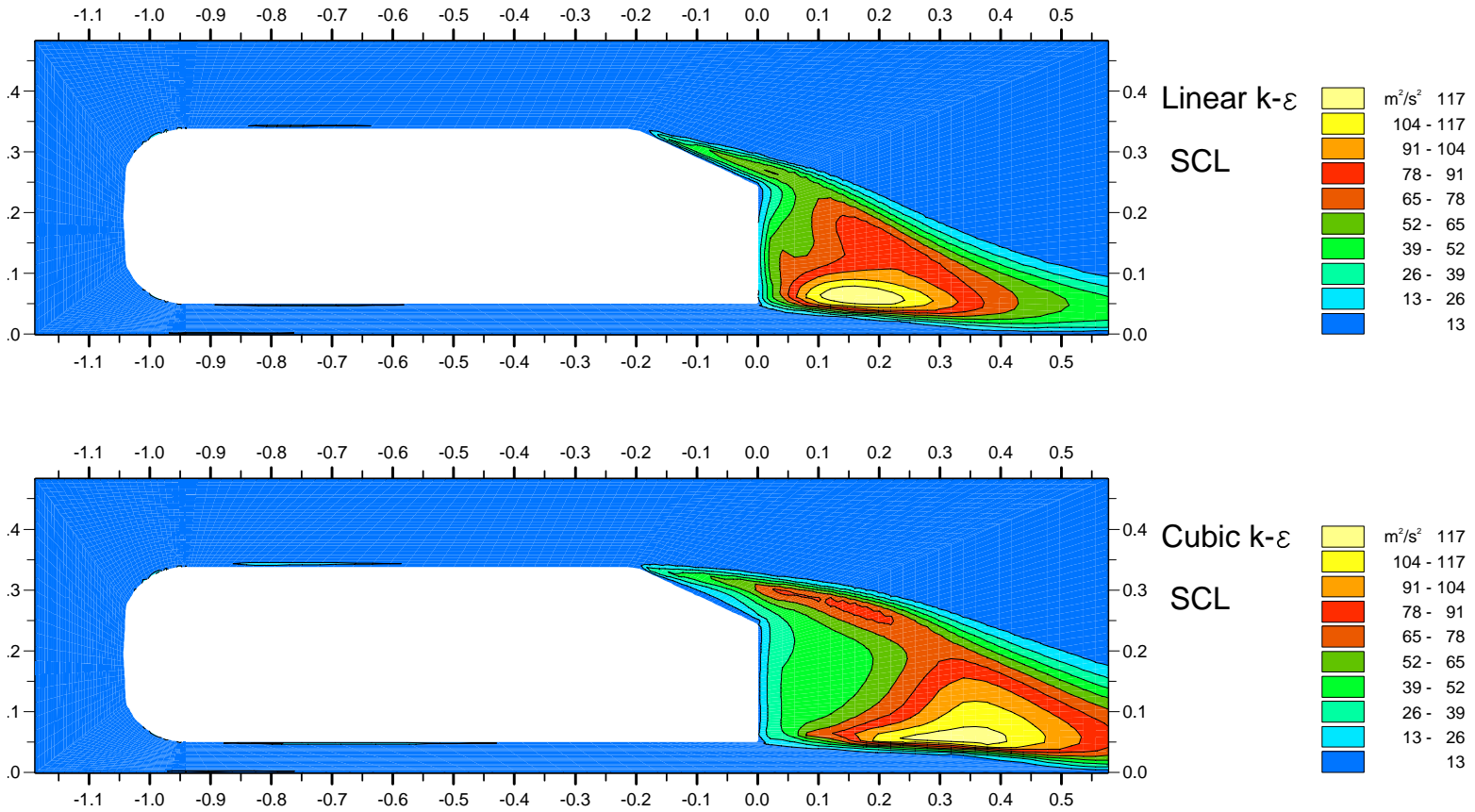


Figure 5: Kinetic energy contours at the centreline ($y = 0$) around the 25° Ahmed body using the linear $k-\varepsilon$ and cubic non-linear $k-\varepsilon$ models with simplified Chieng & Launder wall functions.

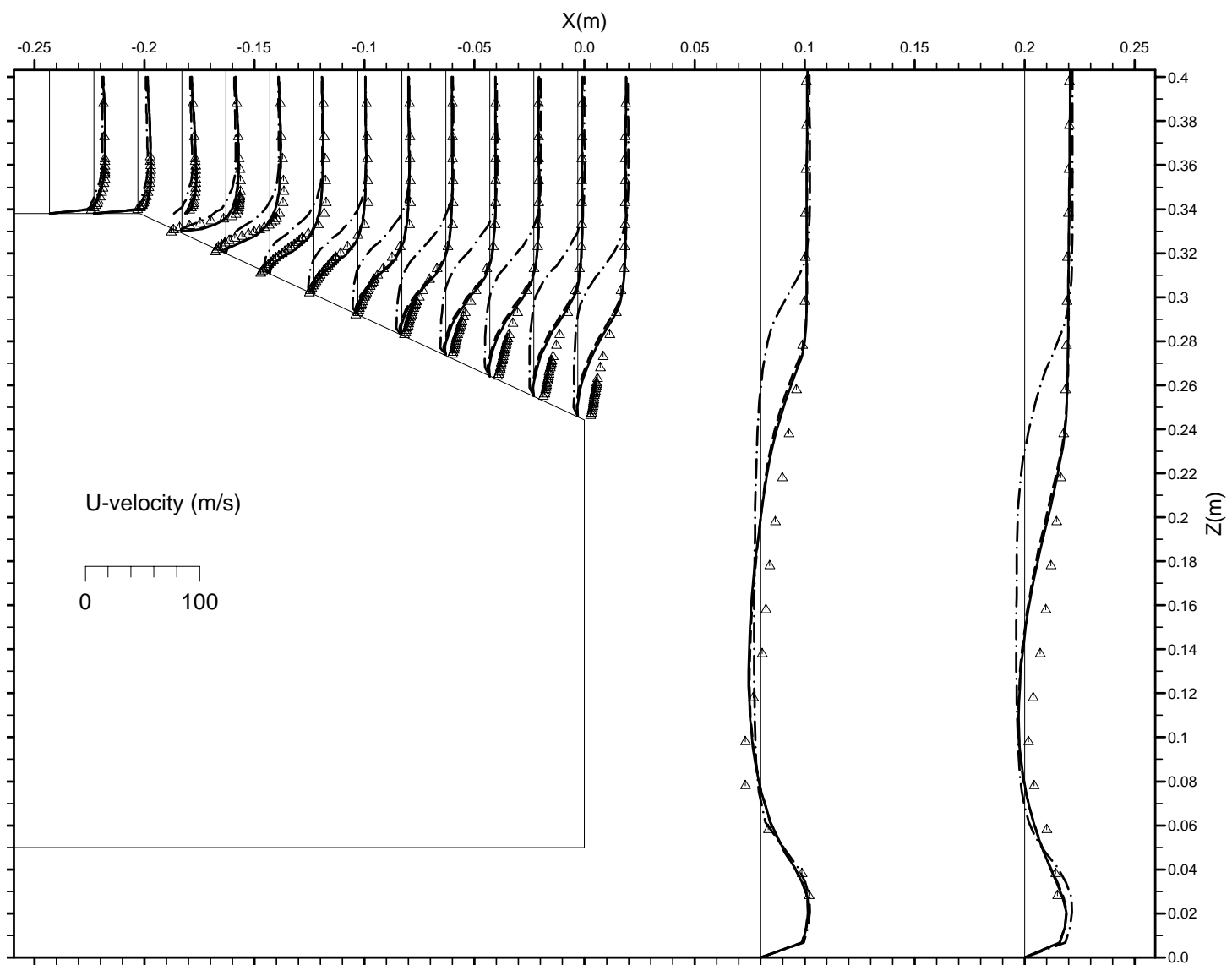


Figure 6: Streamwise U -velocity profiles over the 25° Ahmed body at the centreline ($y = 0$), \cdots : linear $k-\epsilon$ model with SCL; $-\cdot-$: linear $k-\epsilon$ model with AWF; $-$: cubic non-linear $k-\epsilon$ model with SCL; Δ : LSTM experimental data.

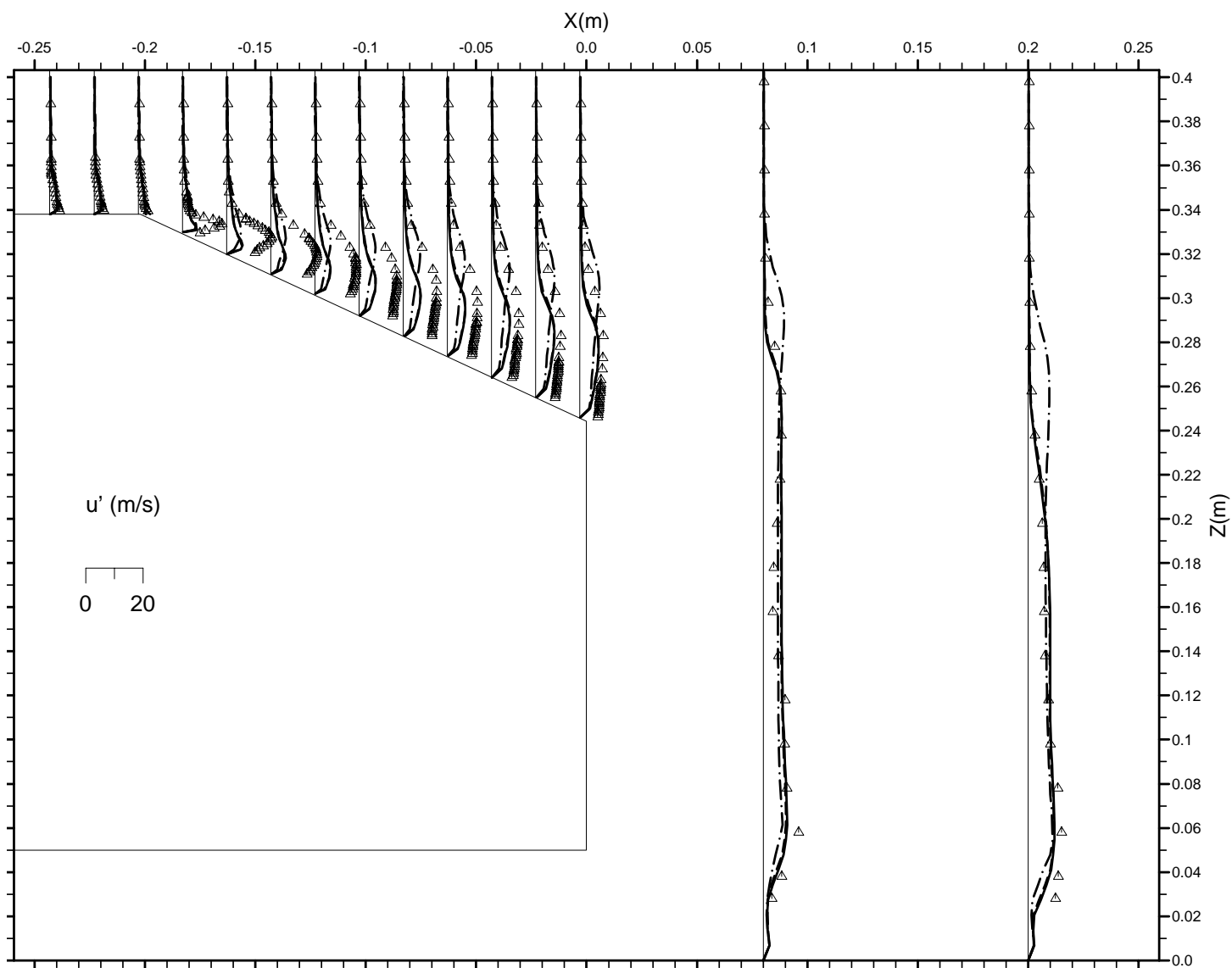


Figure 7: Streamwise \overline{uu} -stress profiles over the 25° Ahmed body at the centreline ($y = 0$), —: linear $k-\epsilon$ model with SCL; - - : linear $k-\epsilon$ model with AWF; — - : cubic non-linear $k-\epsilon$ model with SCL; Δ LSTM experimental data.

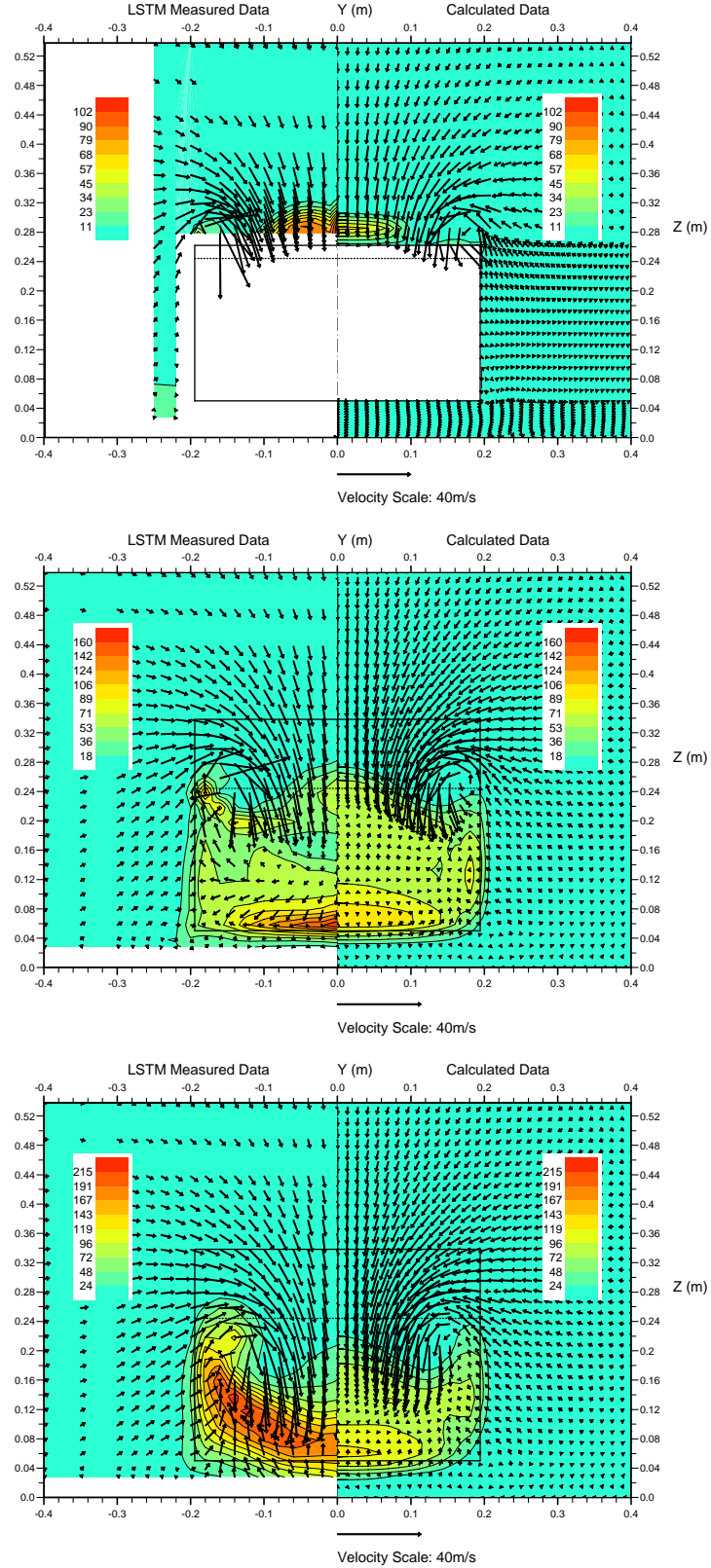


Figure 8: Turbulent kinetic energy contours and secondary velocity vectors for the 25° Ahmed body in three planes at $X = -0.038m$ (top), $X = 0.080m$ (middle) and $X = 0.200m$ (bottom). The left half of the plot shows LSTM experimental data and the right side are calculated results using the linear $k-\varepsilon$ model with the simplified Chieng & Launder wall function.

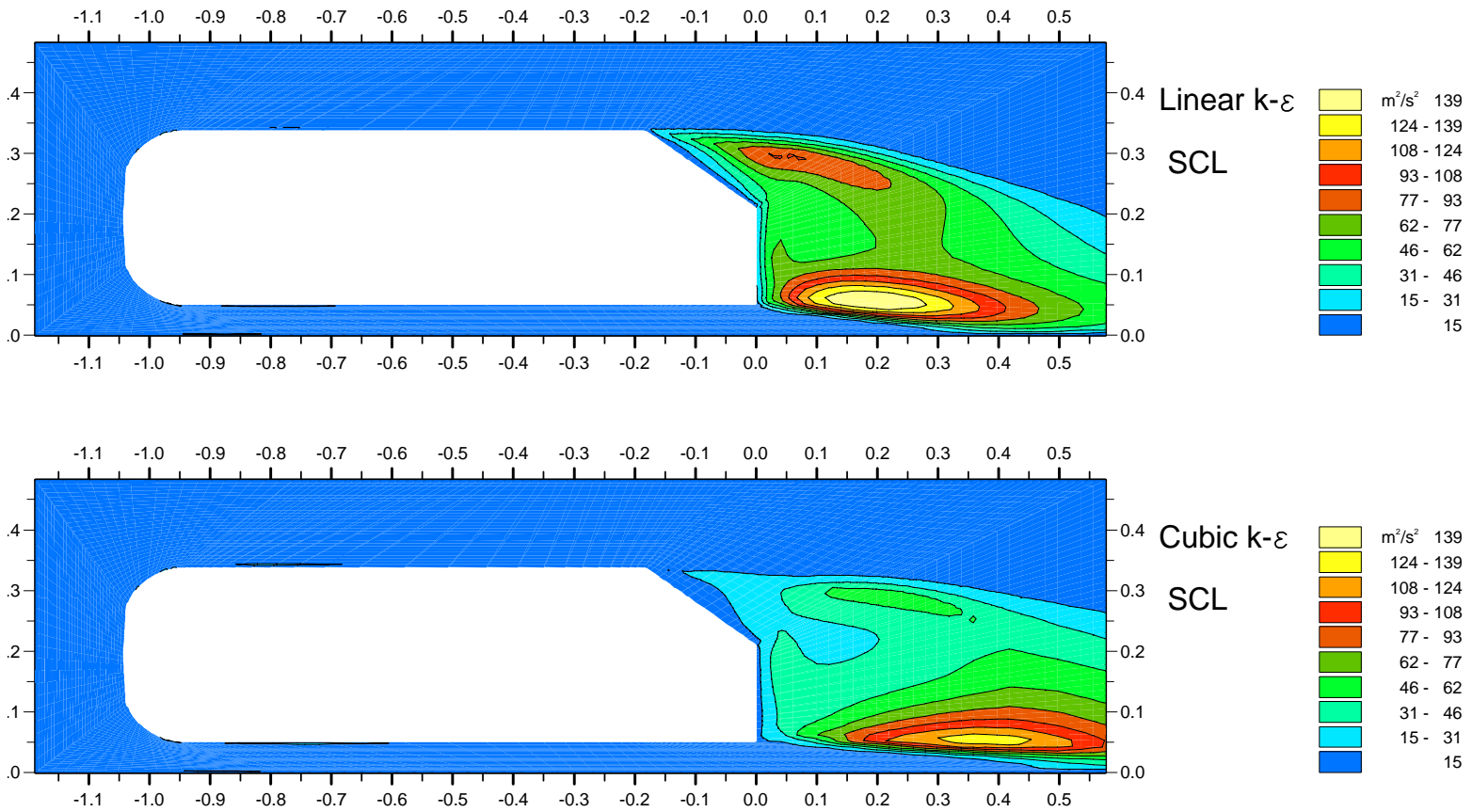


Figure 9: Kinetic energy contours at the centreline ($y = 0$) around the 35° Ahmed body using the linear $k-\varepsilon$ and cubic non-linear $k-\varepsilon$ models with simplified Chieng & Launder wall functions.

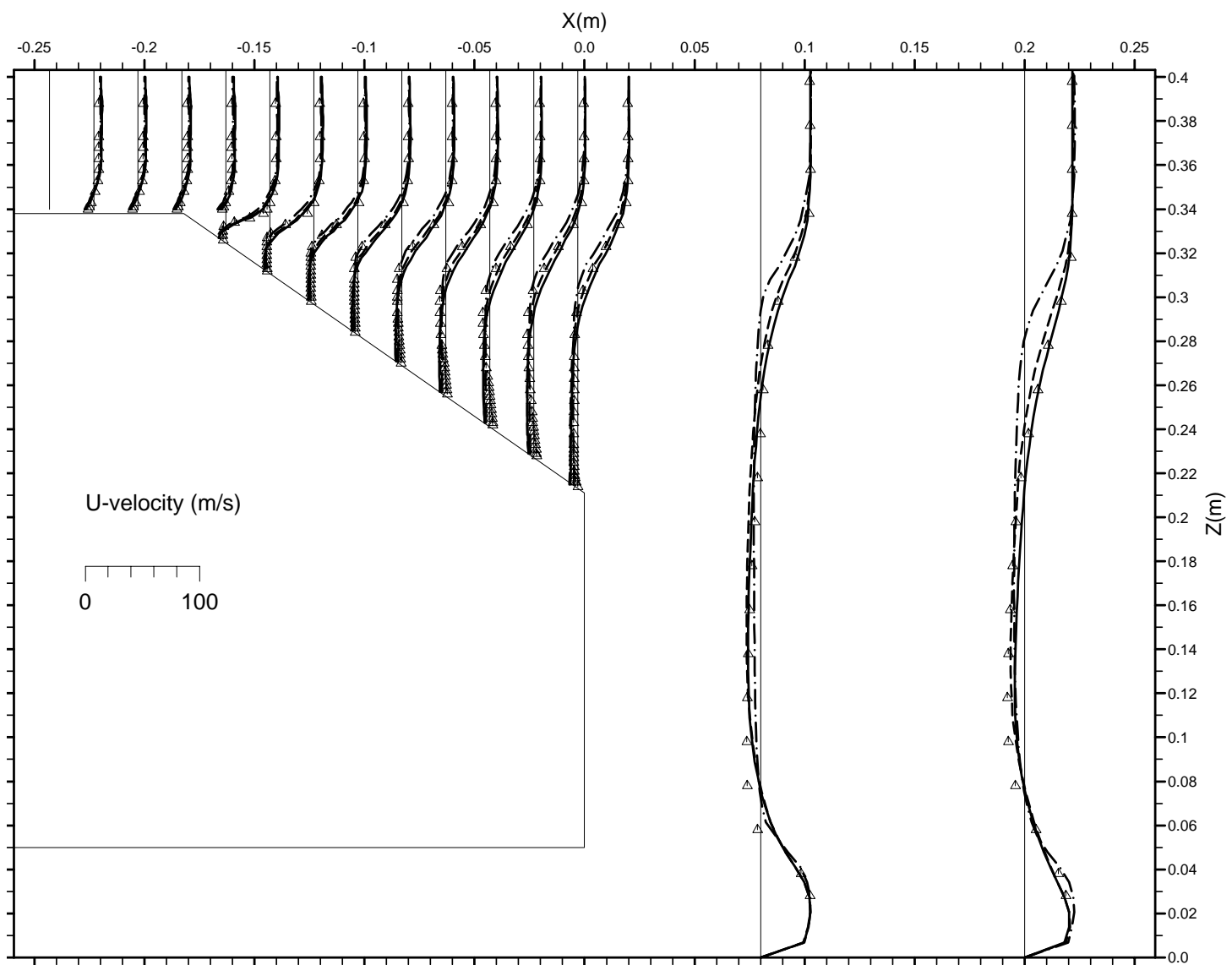


Figure 10: Streamwise U -velocity profiles over the 35° Ahmed body at the centreline ($y = 0$), —: linear $k-\epsilon$ model with SCL; - - : linear $k-\epsilon$ model with AWF; - - - : cubic non-linear $k-\epsilon$ model with SCL; Δ LSTM experimental data.

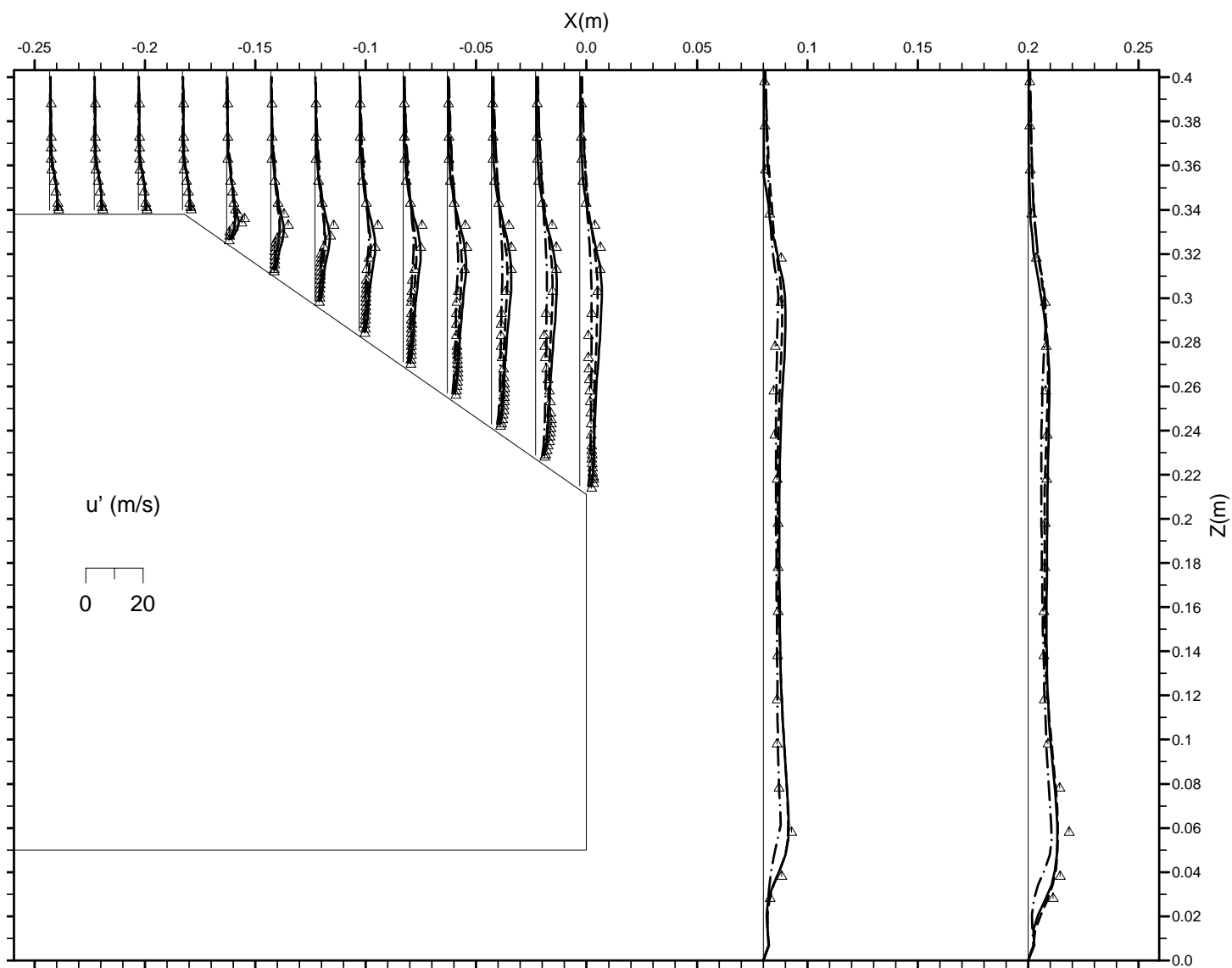


Figure 11: Streamwise \overline{uu} -stress profiles over the 35° Ahmed body at the centreline ($y = 0$), —: linear $k-\epsilon$ model with SCL; - - : linear $k-\epsilon$ model with AWF; - - - : cubic non-linear $k-\epsilon$ model with SCL; Δ LSTM experimental data.

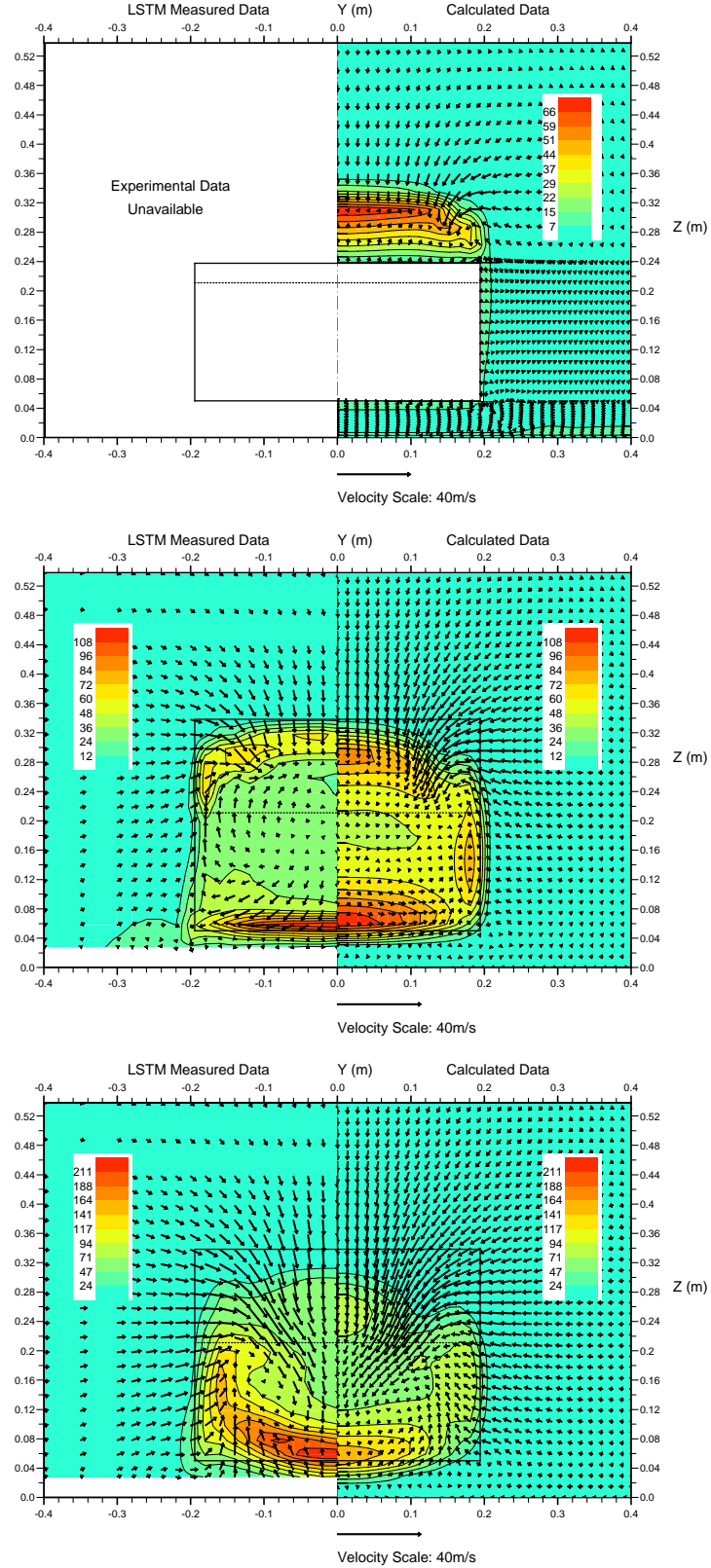


Figure 12: Turbulent kinetic energy contours and secondary velocity vectors for the 35° Ahmed body in three planes at $X = -0.038\text{m}$ (top), $X = 0.080\text{m}$ (middle) and $X = 0.200\text{m}$ (bottom). The left half of the plot shows LSTM experimental data and the right side are calculated results using the linear $k-\varepsilon$ model with the simplified Chieng & Launder wall function.

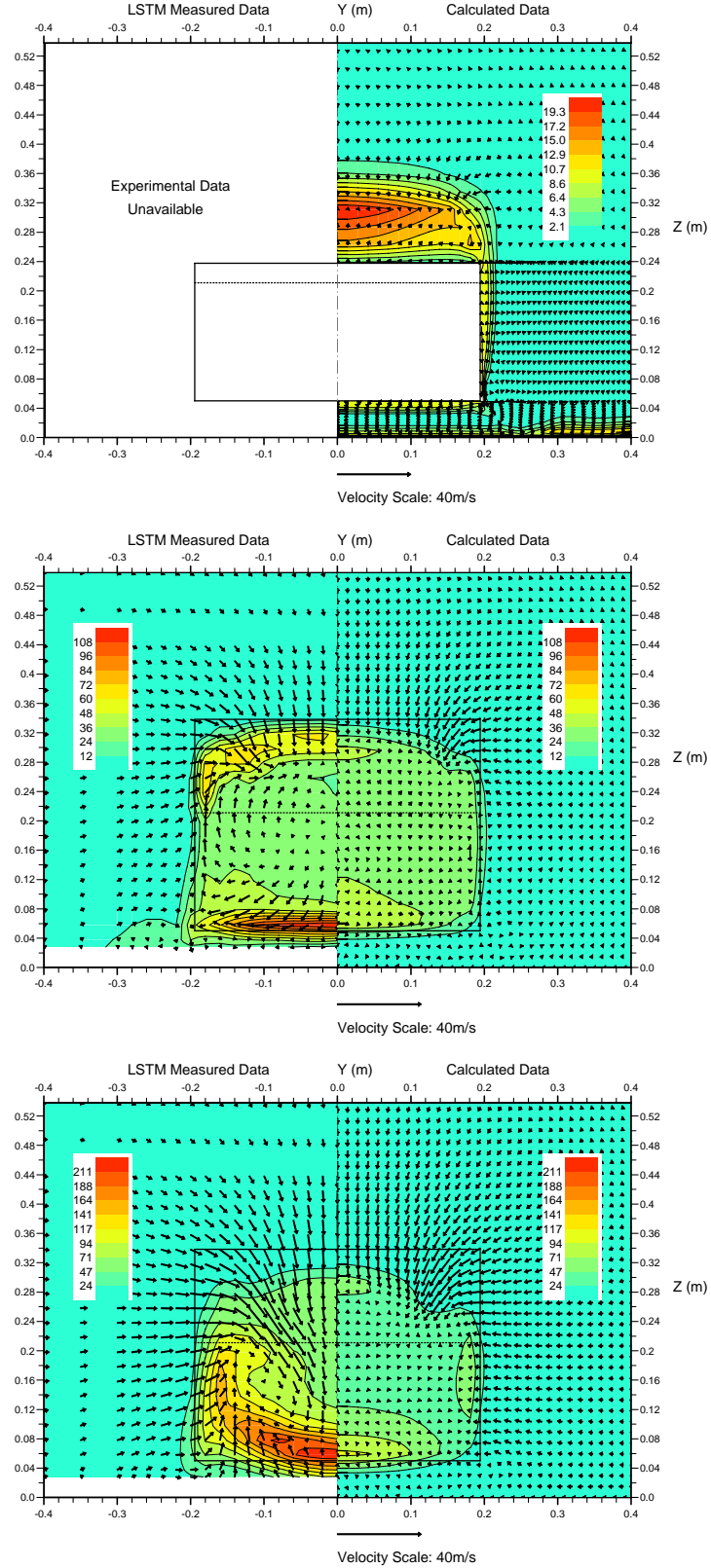


Figure 13: Turbulent kinetic energy contours and secondary velocity vectors for the 35° Ahmed body in three planes at $X = -0.038\text{m}$ (top), $X = 0.080\text{m}$ (middle) and $X = 0.200\text{m}$ (bottom). The left half of the plot shows LSTM experimental data and the right side are calculated results using the cubic non-linear $k-\varepsilon$ model with the simplified Chieng & Launder wall function.